Available online at www.sciencedirect.com
ScienceDirect
Tectonophysics 451 (2008) 71–96
TECTONOPHYSICS
www.elsevier.com/locate/tecto

U-Pb zircon geochronology of late Neoproterozoic–Early Cambrian granitoids in Iran: Implications for paleogeography, magmatism, and exhumation history of Iranian basement

Jamshid Hassanzadeh [a,e,*], Daniel F. Stockli [b], Brian K. Horton [c,e], Gary J. Axen [d,e], Lisa D. Stockli [b], Marty Grove [e], Axel K. Schmitt [e], J. Douglas Walker [b]

[a] School of Geology, University College of Science, University of Tehran, P.O. Box 14155-6455, Tehran, Iran
[b] Department of Geology, University of Kansas, Lawrence, Kansas 66045, USA
[c] Institute for Geophysics and Department of Geological Sciences, Jackson School of Geosciences, University of Texas, Austin, Texas 78712-0254, USA
[d] Department of Earth and Environmental Science, New Mexico Institute of Mining and Technology, Socorro, New Mexico 87801, USA
[e] Department of Earth and Space Sciences, University of California, Los Angeles, California 90095-1567, USA

Received 15 October 2007; accepted 6 November 2007
Available online 15 December 2007

Abstract

Eurasia has largely grown to its present enormous size through episodic addition of crustal blocks by recurring birth and demise of oceans such as Paleotethys and Neotethys. Excluding the Kopet Dagh Mountains in the northeast, crystalline basement rocks of various dimensions are exposed in all continental tectonic zones of Iran. These rocks have traditionally been viewed as continental fragments with Gondwanan affinity and summarily been assigned Precambrian or younger ages, despite the fact that evidence from isotopic dating has largely been lacking. This study presents new ion microprobe and thermal-ionization zircon U-Pb geochronological data from granitoids and orthogneisses from several locations in central Iran and the Sanandaj–Sirjan structural zones to determine crystallization ages and investigate the origin and continental affinity of these various crustal fragments. The resulting U-Pb crystallization ages for the granites and orthogneisses range from late Neoproterozoic to Early Cambrian, matching the mostly juvenile Arabian–Nubian shield and Peri-Gondwanan terranes constructed after the main phase of Pan-African orogenesis. TIMS analyses of zircons with inherited cores from western Iran suggest that the Neoproterozoic crust of Iran might not be entirely juvenile, pointing to the potential presence of inherited older Proterozoic components as is common in the eastern Arabian shield. More importantly, the new zircon U-Pb crystallization ages unequivocally demonstrate that crystalline basement underlying the Sanandaj–Sirjan zone, central Iran, and the Alborz Mountains is composed of continental fragments with Gondwanan affiliation, characterized by wide spread late Neoproterozoic subduction-related magmatism. The exposure of these late Neoproterozoic–Early Cambrian basement rocks in the Iranian regions north of the Zagros is structurally controlled and linked to both large-scale crustal extension and exhumation during Mesozoic and Tertiary time as well as Tertiary collisional tectonics associated with the closure of Neotethys.

Keywords: U-Pb dating; Zircon; Gondwana; Doran granite; Exhumation; Continental basement

1. Introduction

Most paleogeographic and plate tectonic reconstructions for the margin of Gondwana facing the Paleo- and Neotethys oceans propose that crustal blocks making up the collage of Iranian microplates rifted away from Gondwana during the Paleozoic (e.g., Stampfli, 2000; Stampfli et al., 2001). In these reconstructions, a series of crustal fragments separated from the northern margin of Gondwana during the opening of Paleotethys, forming what is referred to as the Cimmerian superterrane. Subsequently, the individual fragments of this Cimmerian superterrane, such as the Sanandaj–Sirjan, Alborz, central Iranian, and Lut blocks were

* Corresponding author. Department of Earth and Space Sciences, University of California, Los Angeles, California 90095-1567, USA.
E-mail address: jamshidh@khayam.ut.ac.ir (J. Hassanzadeh).

0040-1951/$ - see front matter © 2008 Published by Elsevier B.V.
doi:10.1016/j.tecto.2007.11.062

accreted to Laurasia during the Cimmerian orogeny as the result of northward subduction and closure of Paleotethys and the synchronous opening of the Neotethys in the Late Triassic (Sengör, 1987; Stampfli, 2000). The crustal Iranian blocks were assigned a Gondwanan affinity based on flora and excellent correlation of Paleozoic facies with basins in Arabia or India (e.g., Ghavidel-Syooki, 1995; Stampfli, 2000). However, there is little geochronological or isotopic evidence that clearly ties Iranian crustal fragments to the original northern margin of Gondwana.

Historically, the National Iranian Oil Company compiled the first geologic map of Iran in 1959, identifying patches of granitic and orthogneissic basement rocks that crop out in many places in northern, central, and east-central Iran. These blocks were tentatively assigned a Precambrian age and viewed as analogs of the Precambrian basement rocks exposed in the Arabian shield (e.g., Stöcklin, 1968). However, the ages of these rocks have remained poorly constrained and controversial. Reported crystallization ages have ranged from Archean (Haghipour, 1981) to Early Proterozoic (Nadimi, 2007), Middle Proterozoic (Crawford, 1977) and Late Proterozoic (Samani et al., 1994; Davoudzadeh, 1997), based on little or no solid geochronological foundation. However, these age estimates have directly influenced paleogeographic and plate tectonic reconstructions, illustrating the need for robust isotopic age data. Earlier attempts at dating ancient granites in Iran employed available techniques deemed appropriate at the time, such as Rb-Sr (e.g., Crawford, 1977) and K-Ar (e.g., Rachidnejad-Omran et al., 2002), but were unsuccessful in revealing the igneous crystallization ages because of complex and protracted thermal histories and post-intrusive metamorphism (Faure and Mensing, 2005). Modern ion-microprobe and thermal-ionization (TIMS) zircon U-Pb geochronology used in the present study are the preferred methods for determining crystallization ages of granitic magmas due to the closure temperature of the U-Pb system well in excess of the solidus >700–750 °C and the refractory nature of zircon. Thus far, only very sparse published U-Pb zircon age data have been available. Samani et al. (1994) presented the first TIMS U-Pb ages, although discordant, for the Precambrian units in east-central Iran. Ramezani (1997) and Ramezani and Tucker (2003) carried out the first extensive research on Iran basement complexes employing TIMS U-Pb zircon dating of a correlative suite of rocks in central Iran. More recently, ion-microprobe zircon U-Pb dating of plutons in the Alborz Mountains by Axen et al. (2001), Lam (2002), and

Table 1
Sample information for twenty Neoproterozoic–Early Cambrian granitoids and granite mylonites from Iran included in this study

No.	Locality, Sample ID	GPS coordinates			Rock type	Age (Ma)‡
		N (deg, min)	E (deg, min)	Elevation (m)		
Soltanieh Mountains, east and south of Zanjan						
1	ZJ3, Sarv-e Jahan	36° 15.605′	48° 57.657′	2270	Equi-granular beige leucogranite	559
2	ZJ4, Sarv-e Jahan	36° 15.586′	48° 57.822′	2220	Foliated biotite granite, chloritized	544
3	ZJ11, Khorram Darreh*	36° 26.450′	48° 36.620′	2040	Equi-granular biotite granite	53.4
4	ZJ2, Doran*	36° 36.031′	48° 23.105′	1860	White leucogranite	2.8
5	ZJ10, west of Doran	36° 36.103′	48° 20.905′	1835	Argillized leucogranite	567
Takab-west Zanjan region						
6	MoEs24, Moghanlou**	36° 39.100′	47° 55.500′	2235	Biotite granite mylonite	548
7	ZJ9, Mahneshan*	36° 41.890′	47° 33.950′	2050	Biotite granite mylonite	568
Northwestern Sanandaj–Sirjan zone						
8	Bubaktan	36° 15.157′	45° 59.391′	1685	Foliated biotite granite	544
9	Sheikh Chupan	36° 13.545′	45° 54.228′	1783	Biotite granodiorite	551
Muteh gold mine & Varzaneh area, north Golpaygan region						
10	06MT10, Chah Khatoon	33° 42.253′	50° 45.436′	2130	Beige leucogranite	578
11	06MT11B, Chah Khatoon	33° 42.253′	50° 45.436′	2130	Biotite granite	596
12	06MT24, North Varzaneh	33° 37.744′	50° 31.056′	1918	Biotite granite mylonite	588
Torud, Khār Turan & Band-e Hezar Chāh, northeast central Iran						
13	TO40, N. Shotor Kuh, NE of Torud	35° 46.653′	55° 20.940′	1430	Biotite granite mylonite	566
14	EaBi 1a, W. Kuh-e Molhedou***	35° 56.620′	55° 52.708′	1414	Foliated leucogranite	551
15	EaBi22, S. Kuh-e Molhedou	35° 56.600′	56° 02.917′	1230	Biotite-garnet granite mylonite	556
16	EaBi32, Kuh-e Sefid Sang	35° 50.667′	55° 45.383′	1350	Biotite granite	554
17	EaBi 125, Delbar, SE Kuh-e Molhedou	35° 58.833′	56° 04.717′	1177	Foliated leucogranite	534
18	G227, W. Kuh-e Molhedou***	35° 54.100′	55° 54.267′	1316	Biotite-garnet granite	522
19	TO46, Band-e Hezar Chāh	36° 00.517′	55° 34.867′	1491	Pink foliated leucogranite	581
20	TO50, Band-e Hezar Chāh	35° 57.534′	55° 32.757′	1645	Biotite granite mylonite	601
21	TO-He4, Band-e Hezar Chāh	36° 00..900′	55° 31.402′	1780	Leucogranite mylonite	572
Lahijan area, northern west Alborz mountains (after Lam, 2002)						
22	LJ6, Leila Kuh, SW Langarud*	37° 009.900′	50° 07.400′	210	Pink biotite granite	551

The Pliocene phase in the Doran intrusive complex and the Eocene Khorram Darreh granite dated in this study are also shown.
Notes: ‡See Table 2 for details. Rock samples were collected by JH excluding *(JH & DS), **(D. Esmaeily) and ***(A. R. Malekpour).

Guest et al. (2006) provided a first glimpse of the complex magmatic evolution of the Alborz Mountains, with zircon U-Pb ages yielding late Neoproterozoic, Cretaceous, Eocene, and Miocene ages.

In an attempt to shed light on the paleogeographic evolution of Iran and to elucidate the nature of the purported Precambrian granitic and orthogneissic basement in Iran, this paper presents new ion-microprobe and TIMS U-Pb zircon crystallization ages from twenty-one rock samples from five different areas in central Iran and the Sanandaj–Sirjan zone (Table 1). For the Lahijan granite, northern Alborz, unpublished data of Lam (2002), generated in the same ion-probe lab, is incorporated. This new geochronological dataset, in combination with field observations and data from published studies, is used to clarify the magmatic evolution of the Iranian continental basement and to investigate the possible implications for paleogeography, ore deposits, and exhumation history of Iranian continental crust.

2. U-Pb geochronology

2.1. Ion-microprobe zircon U-Pb geochronology

Table 1 provides the pertinent sample information and locations for all samples dated in this study. Table 2 summarizes the data from ion microprobe isotopic analyses performed on twenty rock specimens collected from different granitoid plutons and orthogneissic/mylonitic complexes of Iran. All of the reported ion-microprobe zircon U-Pb ages are based on U, Pb, and Th isotopic measurements employing spot analysis using the Cameca IMS 1270 ion microprobe at the University of California, Los Angeles (UCLA). Analytical methods follow the procedures described by Quidelleur et al. (1997) and Schmitt et al. (2003a,b). Following mineral separation using conventional liquid and magnetic techniques, zircon grains were hand selected, mounted in epoxy, and coated with ~100 Å of gold. The ion-microprobe spot analyses utilized a primary ion beam focused to an ~30 μm diameter spot and a secondary ion beam with a mass resolving power of 5000 and energy window of 50 eV. Following a pre-sputtering period of ~180 s, each analysis collected data for 8–10 cycles. The sample chamber was flooded with oxygen at $\sim 3\times10^{-5}$ Torr to enhance secondary Pb^{+} ionization. The reported weighted-mean ages are based on $^{206}Pb/^{238}U$ ages calculated using zircon standard AS3 (1099±0.5 Ma; Paces and Miller, 1993). Common lead corrections were made using the measured values of ^{204}Pb (Stacey and Kramers, 1975) and the values of ^{208}Pb corrected for ^{232}Th-derived ^{208}Pb (Compston et al., 1984), which are considered a proxy for common ^{206}Pb and ^{207}Pb. These corrections use the anthropogenic Pb compositions reported for the Los Angeles basin (Sanudo-Wilhelmy and Flegal, 1994). All age uncertainties are reported at the 95% level (Table 2).

2.2. Thermal-ionization (TIMS) zircon U-Pb geochronology

Given the reconnaissance nature of our study in trying to shed light on the timing and spatial distribution of Neoproterozoic magmatism in Iran, we predominantly relied on ion-microprobe U-Pb dating. However, in three cases we employed TIMS U-Pb geochronology, to gain a more precise insight into the intrusion age and inherited zircon component of the Doran granite. TIMS U-Pb analyses were carried out at the University of Kansas. Single and multi-grain zircon samples were carefully hand-selected and air-abraded to reduce radiogenic lead loss following the procedures outlined by Krogh (1982). Pressure-vessel HF-HNO_3 dissolution followed the methods of Krogh (1973) and Parrish (1987). Elemental separation was carried out using an HCl anion column chemistry protocol for separating lead and uranium. Isotopic analyses were determined on a VG Sector multicollector thermal ionization mass spectrometer. A mass fractionation correction of 0.16%±0.05%/amu, as determined by standard runs on NBS 981 (common lead) and NBS 982 (equal atom lead), was applied to the lead data. A mass fractionation of 0.10%±0.05%/amu, as determined by standard runs on U500, was applied to the U data. Samples were spiked with a mixed $^{205}Pb/^{235}U$ spike. Errors on $^{206}Pb/^{204}Pb$ were minimized by use of a Daly multiplier and are typically on the order of 1% or less. Common lead corrections were made using values determined from Stacey and Kramers (1975) for the interpreted crystallization age. Decay constants used were $^{238}U=0.15513\times10^{-9}$ yr^{-1} and $^{235}U=0.98485\times10^{-9}$ yr^{-1} (Steiger and Jager, 1977). All individual analyses are reported in Table 3 (uncertainties at the 2σ level).

3. Geological setting

Iran is constructed chiefly of continental fragments initially rifted from Gondwana as Paleotethys and Neotethys oceans opened, then later re-amalgamated as both oceans closed (Berberian and King, 1981; Sengör, 1987). The major tectonic provinces of western and central Iran (Fig. 1) include, from north to south: the Alborz mountains, a variety of small blocks composing central Iran, the Urumieh–Dokhtar arc, the Sanandaj–Sirjan zone, the Zagros mountains, and the Zagros foreland (Arabian shield). Despite their varied histories, the continental fragments composing Iran share a relatively similar stratigraphic record of mostly shallow-marine sedimentation from late Neoproterozoic to Permian time (Stöcklin, 1968). The principal tectonic provinces are separated by two major suture zones representing closure of Paleotethys and Neotethys oceans.

Paleotethys Ocean closed during collision of Iran and the Eurasian part of Pangea in the Late Triassic (Alavi et al., 1997; Stampfli, 2000). Although the suture position is accurately known along the trend of the Kopet Dagh and Caucasus mountains, it may proceed either continuously (Stöcklin, 1974; Ruttner, 1993; Davoudzadeh, 1997) or discontinuously (Sengör, 1990) along the northern flank of the Alborz mountains of northern Iran. Where exposed, the suture is overlapped by Upper Triassic–Lower Jurassic nonmarine deposits of the Shemshak Formation, presumably derived from the Eurasian part of Pangea to the north (Dercourt et al., 1986).

The subduction of the Neotethys Ocean had a complex history involving collision of Arabia with Iran and growth of the Zagros Mountains. Stampfli and Borel (2004) suggested that the Iran portion of the Neotethys was already closed in the late Cretaceous, following obduction along the Arabian margin,

Table 2
Iran zircon U-Pb ion-microprobe data

Sample ID	$^{207}Pb^*/^{235}U$	Error $^{207}Pb^*/^{235}U$ 1 σ %	$^{206}Pb^*/^{238}U$	Error $^{206}Pb^*/^{238}U$ 1 σ %	Error corr	$^{207}Pb^*/^{206}Pb^*$	Error $^{207}Pb^*/^{206}Pb^*$ 1 σ %	Age (Ma) $^{206}Pb/^{238}U$	Age (Ma) $^{206}Pb/^{238}U$ 1 σ	Age (Ma) $^{207}Pb/^{235}U$	Age (Ma) $^{207}Pb/^{235}U$ 1 σ	Age (Ma) $^{207}Pb/^{206}Pb$	Age (Ma) $^{207}Pb/^{206}Pb$ 1 σ
ZJ3, Sarv-e Jahan, east Soltanieh mountains													
g1	0.74900	5.63	0.09714	6.21	0.879	0.05592	2.96	597.6	35.4	567.6	24.5	449.2	66.0
g2	0.78450	6.41	0.09653	7.07	0.919	0.05895	2.79	594.0	40.1	588.0	28.6	565.2	60.9
g3	0.75050	5.47	0.09809	6.17	0.876	0.05549	2.98	603.2	35.5	568.5	23.8	432.0	66.6
Weighted Mean = 599 ± 42 [7%] 95% conf.; MSWD = 0.015													
ZJ4, Sarv-e Jahan, east Soltanieh mountains													
g10	0.63970	3.67	0.07897	4.31	0.799	0.05875	2.60	490.0	20.3	502.1	14.5	557.8	56.9
g8	0.70270	4.20	0.08655	4.25	0.987	0.05889	0.69	535.1	21.8	540.4	17.6	563.0	15.8
g7	0.69150	4.31	0.08702	4.67	0.924	0.05764	1.79	537.9	24.1	533.7	17.9	516.1	39.5
g3	0.66190	4.72	0.08805	8.61	0.651	0.05452	6.60	544.0	44.9	515.8	19.1	392.6	148.0
g6	0.70410	4.28	0.08878	4.39	0.976	0.05752	0.95	548.3	23.1	541.2	17.9	511.5	21.3
g5	0.74270	4.59	0.09286	4.59	0.962	0.05801	1.26	572.4	25.1	564.0	19.9	530.1	28.0
g1	0.76450	4.94	0.09436	5.29	0.875	0.05876	2.58	581.3	29.4	576.6	21.7	558.2	56.4
g2	0.77240	4.73	0.09577	4.85	0.974	0.05849	1.10	589.6	27.3	581.1	20.9	548.2	24.4
Weighted Mean = 544 ± 29 [5.3%] 95% conf.; MSWD = 1.9													
ZJ10, Chevarzagh, central Soltanieh mountains, south of Zanjan, west of Doran													
g9	0.70740	4.41	0.08987	4.63	0.965	0.05708	1.22	554.8	24.6	543.2	18.6	494.6	27.2
g10	0.71250	4.55	0.09019	4.71	0.964	0.05729	1.25	556.7	25.1	546.2	19.2	502.7	28.0
g6	0.74740	4.33	0.09036	4.35	0.961	0.05999	1.21	557.7	23.3	566.7	18.8	603.2	26.6
g7	0.73970	4.61	0.09103	5.03	0.916	0.05893	2.02	561.6	27.1	562.2	19.9	564.5	44.3
g1	0.73200	4.65	0.09272	4.87	0.978	0.05726	1.02	571.6	26.6	557.7	19.9	501.6	22.9
g2	0.75400	4.35	0.09405	4.41	0.979	0.05815	0.90	579.4	24.5	570.5	19.0	535.4	20.1
g8	0.77930	4.87	0.09702	4.98	0.979	0.05826	1.00	596.9	28.4	585.1	21.7	539.6	22.4
Weighted Mean = 567 ± 19 [3.3%] 95% conf.; MSWD = 0.34													
MoEs24, Moghanlou, west Zanjan region													
g2_s2	0.68530	6.47	0.08484	6.60	0.988	0.05858	1.04	524.9	33.3	530.0	26.7	551.5	23.1
g2_s1	0.68780	6.57	0.08617	6.62	0.992	0.05789	0.83	532.8	33.8	531.5	27.2	525.6	18.8
g5_s1	0.67520	9.45	0.08634	10.68	0.948	0.05672	3.47	533.9	54.7	523.9	38.7	480.7	76.9
g4_s4	0.71660	9.21	0.08761	9.38	0.972	0.05932	2.21	541.4	48.7	548.7	39.0	578.9	48.2
g4_s2	0.71980	9.13	0.08966	9.43	0.978	0.05823	1.97	553.5	50.0	550.5	38.8	538.4	43.4
g5_s3	0.70970	8.61	0.08980	9.13	0.937	0.05732	3.19	554.4	48.5	544.6	36.3	503.9	70.4
g1_s1	0.72950	9.48	0.09063	9.57	0.981	0.05837	1.87	559.3	51.3	556.3	40.6	543.7	41.1
g5_s2	0.72790	9.64	0.09066	10.25	0.949	0.05823	3.23	559.4	54.9	555.3	41.2	538.4	70.8
g3_s1	0.71510	9.83	0.09148	10.10	0.971	0.05670	2.40	564.3	54.6	547.8	41.6	479.9	53.2
g4_s3	0.74930	10.74	0.09236	11.06	0.965	0.05884	2.91	569.5	60.3	567.8	46.7	561.2	63.5
g4_s1	0.75370	9.71	0.09405	10.19	0.974	0.05813	2.34	579.4	56.5	570.4	42.4	534.7	51.4
g3_s2	0.74430	10.14	0.09419	10.43	0.969	0.05731	2.58	580.3	57.9	564.9	43.9	503.5	57.0
Weighted Mean = 548 ± 27 [4.9%] 95% conf.; MSWD = 0.16													
ZJ9, Mahneshan, Takab region													
g10	0.56290	9.58	0.07214	9.77	0.984	0.05659	1.73	449.0	42.4	453.4	35.0	475.6	38.5
g7	0.61950	8.64	0.07995	8.83	0.970	0.05620	2.14	495.8	42.1	489.5	33.6	460.3	47.6
g12	0.71670	7.69	0.08817	7.76	0.932	0.05895	2.85	544.7	40.5	548.7	32.6	565.2	62.2
g9	0.71870	7.57	0.08868	7.64	0.990	0.05878	1.05	547.7	40.1	549.9	32.1	559.0	23.4
g2	0.74350	7.51	0.09276	7.52	0.998	0.05813	0.45	571.8	41.1	564.4	32.5	534.7	10.8
g1	0.77840	8.01	0.09622	8.03	0.996	0.05868	0.70	592.2	45.4	584.6	35.6	555.2	15.8

g6_s1	0.78040	7.98	0.09734	8.07	0.984	0.05815	1.45	598.8	46.2	585.7	35.5	535.4	32.2
g6_s2	0.82350	8.97	0.10150	8.93	0.993	0.05882	1.06	623.2	53.0	610.0	41.1	560.4	23.5
g11	0.82890	8.03	0.10280	8.01	0.999	0.05845	0.34	630.8	48.1	613.0	36.9	546.7	8.8
g8	0.87150	8.80	0.10800	8.79	0.999	0.05854	0.39	661.1	55.2	636.4	41.6	550.0	9.7
g4	0.92070	9.26	0.11020	9.53	0.954	0.06057	2.86	673.9	61.0	662.7	45.1	624.0	61.8
Weighted Mean = 568 ± 44 [7.8%] 95% conf.; MSWD = 2.1													
Bubaktan, northwest Sanandaj–Sirjan zone													
g5	0.68330	3.56	0.08487	4.18	0.919	0.05839	1.67	525.1	21.1	528.8	14.7	544.4	36.8
g4	0.69330	3.91	0.08739	4.58	0.893	0.05754	2.07	540.1	23.7	534.8	16.3	512.3	45.7
g2	0.69640	4.50	0.08770	4.69	0.883	0.05759	2.23	541.9	24.4	536.6	18.7	514.2	49.2
g3	0.70420	4.33	0.08827	4.39	0.915	0.05786	1.80	545.3	22.9	541.3	18.2	524.5	39.8
g6	0.71960	3.86	0.08847	4.40	0.945	0.05899	1.47	546.5	23.0	550.4	16.4	566.7	32.4
g1	0.74520	4.24	0.09305	4.55	0.960	0.05808	1.28	573.6	25.0	565.4	18.4	532.8	28.4
Weighted Mean = 544 ± 19 [3.4%] 95% conf.; MSWD = 0.45													
Sheikh Chupan, northwest Sanandaj–Sirjan zone													
g2	0.70200	4.59	0.08787	4.80	0.890	0.05794	2.21	542.9	25.0	540.0	19.2	527.5	48.6
g4	0.70250	4.51	0.08897	5.35	0.842	0.05727	2.89	549.4	28.2	540.3	18.9	501.9	63.7
g3	0.69480	5.06	0.08916	5.12	0.873	0.05652	2.57	550.6	27.0	535.7	21.1	472.9	56.9
g5	0.72070	4.40	0.08981	4.97	0.875	0.05820	2.40	554.4	26.4	551.1	18.7	537.3	52.8
g6	0.72480	4.41	0.09124	7.08	0.635	0.05761	5.47	562.9	38.1	553.5	18.8	515.0	120.1
Weighted Mean = 551 ± 25 [4.5%] 95% conf.; MSWD = 0.055													
MT10, Muteh gold mine, north Golpaygan region													
g2	0.71430	4.54	0.08784	5.18	0.883	0.05897	2.43	542.7	27.0	547.3	19.2	566.0	53.0
g5	0.73070	4.85	0.09258	5.20	0.938	0.05724	1.80	570.8	28.4	557.0	20.8	500.8	40.0
g6	0.75360	4.27	0.09319	4.34	0.947	0.05866	1.41	574.4	23.9	570.3	18.6	554.5	31.1
g3	0.76400	4.53	0.09459	4.65	0.988	0.05858	0.72	582.6	25.9	576.3	19.9	551.5	16.4
g1	0.77690	5.41	0.09595	5.33	0.967	0.05872	1.38	590.6	30.1	583.7	24.0	556.7	30.4
g4	0.79820	4.77	0.09911	4.82	0.988	0.05841	0.74	609.2	28.0	595.8	21.5	545.2	16.8
Weighted Mean = 578 ± 22 [3.7%] 95% conf.; MSWD = 0.65													
MT11B, Muteh gold mine, north Golpaygan region													
g3	0.71380	5.53	0.09043	5.84	0.858	0.05725	3.04	558.1	31.2	547.0	23.4	501.2	67.2
g4	0.73640	4.57	0.09241	4.74	0.968	0.05780	1.18	569.8	25.9	560.3	19.7	522.2	26.4
g5	0.78320	5.18	0.09701	5.55	0.934	0.05855	1.99	596.9	31.6	587.3	23.1	550.4	43.6
g2	0.82210	5.00	0.09920	5.14	0.975	0.06010	1.15	609.7	29.9	609.2	22.9	607.2	25.3
g6	0.81990	4.57	0.10070	4.75	0.965	0.05905	1.25	618.5	28.0	608.0	20.9	568.9	27.5
g1	0.81520	5.24	0.10320	5.36	0.972	0.05729	1.26	633.1	32.3	605.4	23.9	502.7	28.1
Weighted Mean = 596 ± 24 [4%] 95% conf.; MSWD = 0.94,													
MT24, north of Varzaneh, north Golpaygan region													
g1	0.70170	4.99	0.08913	5.76	0.933	0.05710	2.11	550.4	30.4	539.8	20.9	495.4	46.8
g2	0.74540	4.30	0.09370	4.91	0.898	0.05770	2.17	577.4	27.1	565.6	18.6	518.4	47.8
g3	0.78260	4.51	0.09560	4.66	0.950	0.05937	1.46	588.6	26.2	587.0	20.1	580.7	32.1
g4	0.76940	4.33	0.09641	4.70	0.889	0.05788	2.16	593.3	26.6	579.4	19.1	525.2	47.5
g5	0.76720	5.06	0.09883	6.68	0.840	0.05630	3.67	607.5	38.8	578.2	22.3	464.2	81.5
g6	0.80740	4.96	0.10050	5.06	0.916	0.05826	2.06	617.3	29.8	601.0	22.5	539.6	45.2
Weighted Mean = 588 ± 23 [4%] 95% conf.; MSWD = 0.59													

(continued on next page)

Table 2 (*continued*)

Sample ID	$^{207}Pb^*/^{235}U$	Error $^{207}Pb^*/^{235}U$ 1 σ %	$^{206}Pb^*/^{238}U$	Error $^{206}Pb^*/^{238}U$ 1 σ %	Error corr	$^{207}Pb^*/^{206}Pb^*$	Error $^{207}Pb^*/^{206}Pb^*$ 1 σ %	Age (Ma) $^{206}Pb/^{238}U$	Age (Ma) $^{206}Pb/^{238}U$ 1 σ	Age (Ma) $^{207}Pb/^{235}U$	Age (Ma) $^{207}Pb/^{235}U$ 1 σ	Age (Ma) $^{207}Pb/^{206}Pb$	Age (Ma) $^{207}Pb/^{206}Pb$ 1 σ
TO 40, Shotor Kuh, NE Torud, NE central Iran													
g8	0.65900	4.53	0.08217	5.23	0.820	0.05817	3.00	509.1	25.6	514.0	18.3	536.2	65.8
g3	0.68870	4.79	0.08931	6.47	0.745	0.05593	4.32	551.5	34.2	532.0	19.9	449.6	96.0
g6	0.74150	5.07	0.08998	6.72	0.750	0.05977	4.45	555.4	35.8	563.3	21.9	595.3	96.4
g2	0.73430	4.95	0.09357	6.10	0.838	0.05692	3.33	576.6	33.6	559.1	21.3	488.4	73.6
g7	0.74070	5.33	0.09406	6.00	0.961	0.05711	1.72	579.5	33.3	562.8	23.0	495.8	38.2
g1	0.78070	5.70	0.09660	6.60	0.884	0.05861	3.09	594.5	37.5	585.9	25.4	552.6	67.6
g4	0.76390	5.12	0.09803	5.47	0.953	0.05652	1.66	602.9	31.5	576.3	22.5	472.9	36.9
g5	0.80300	5.75	0.10030	7.12	0.853	0.05806	3.73	616.2	41.8	598.5	26.0	532.0	81.8
Weighted Mean = 566 ± 31 [5.5%] 95% conf.; MSWD = 1.3													
EaBi1A, Khar Turan area, NE central Iran													
g5	0.69450	3.64	0.08673	4.03	0.885	0.05808	1.88	536.2	20.7	535.5	15.2	532.8	41.3
g6	0.70580	4.01	0.08834	4.19	0.966	0.05795	1.09	545.7	21.9	542.2	16.9	527.9	24.2
g4	0.73820	4.67	0.08953	5.34	0.854	0.05980	2.78	552.8	28.3	561.4	20.1	596.3	60.5
g3	0.70980	4.23	0.09025	5.87	0.786	0.05704	3.65	557.0	31.3	544.6	17.8	493.1	80.6
g1	0.72320	4.56	0.09047	4.81	0.948	0.05798	1.53	558.3	25.7	552.6	19.4	529.0	33.9
g2	0.70640	4.07	0.09151	4.48	0.904	0.05599	1.92	564.5	24.2	542.6	17.1	452.0	42.9
Weighted Mean = 551 ± 20 [5.5%] 95% conf.; MSWD = 0.20													
EABi22, Khar Turan area, NE central Iran													
g3	0.65710	7.60	0.08268	7.64	0.981	0.05764	1.49	512.1	37.6	512.8	30.6	516.1	32.9
g6_s2	0.73050	8.74	0.08752	9.14	0.977	0.06053	1.95	540.9	47.4	556.8	37.5	622.6	42.3
g2_s2	0.75600	8.44	0.09015	8.40	0.988	0.06082	1.29	556.4	44.8	571.7	36.9	632.9	28.2
g6_s1	0.71410	8.61	0.09028	8.63	0.986	0.05737	1.43	557.2	46.0	547.2	36.4	505.8	31.7
g4	0.74330	8.65	0.09111	8.66	0.994	0.05917	0.94	562.1	46.6	564.3	37.4	573.4	20.9
g1	0.75500	8.77	0.09229	8.82	0.991	0.05933	1.15	569.1	48.0	571.1	38.3	579.2	25.5
g6_s3	0.73050	8.64	0.09229	8.62	0.987	0.05740	1.38	569.1	47.0	556.8	37.0	506.9	30.6
g5	0.73410	9.14	0.09235	9.39	0.978	0.05765	1.98	569.4	51.2	559.0	39.3	516.5	43.7
g2_s1	0.77300	8.23	0.09624	8.24	0.998	0.05825	0.53	592.3	46.6	581.5	36.4	539.2	12.5
Weighted Mean = 556 ± 30 [5.4%] 95% conf.; MSWD = 0.29													
EaBi32, Khar Turan area, NE central Iran													
g5	0.67690	7.88	0.08536	7.95	0.986	0.05751	1.32	528.0	40.3	524.9	32.3	511.1	29.3
g2_s2	0.70630	8.50	0.08814	8.82	0.970	0.05812	2.15	544.5	46.1	542.5	35.7	534.3	47.3
g2-s1	0.71350	8.54	0.09112	8.66	0.984	0.05679	1.55	562.2	46.6	546.8	36.1	483.4	34.6
g6	0.71290	8.98	0.09175	9.10	0.989	0.05635	1.38	565.9	49.3	546.5	38.0	466.2	30.8
g3	0.76460	8.13	0.09390	8.17	0.996	0.05906	0.71	578.6	45.2	576.7	35.8	569.3	16.0
Weighted Mean = 554 ± 40 [7.2%] 95% conf.; MSWD = 0.21													
EaBi125, Khar Turan area, NE central Iran													
g4	0.62330	3.50	0.07959	3.93	0.878	0.05680	1.88	493.7	18.7	491.9	13.7	483.8	41.8
g6	0.68770	4.04	0.08570	4.13	0.971	0.05820	0.99	530.1	21.0	531.4	16.7	537.3	22.2
g5	0.69620	4.00	0.08736	4.27	0.957	0.05780	1.24	539.9	22.1	536.5	16.7	522.2	27.6
g3	0.70450	4.22	0.08760	4.45	0.935	0.05833	1.58	541.3	23.1	541.5	17.7	542.2	34.8
g2	0.71840	4.39	0.08898	4.39	0.964	0.05855	1.17	549.5	23.1	549.7	18.6	550.4	26.0
g1	0.73970	4.76	0.09486	4.68	0.976	0.05656	1.03	584.2	26.2	562.2	20.5	474.4	23.2
Weighted Mean = 534 ± 31 [5.8%] 95% conf.; MSWD = 1.8													

G227, Khar Turan area, NE central Iran													
g5	0.66500	6.05	0.08131	6.63	0.919	0.05932	2.61	503.9	32.1	517.7	24.5	578.9	57.0
g7	0.65620	6.29	0.08190	6.39	0.977	0.05811	1.36	507.5	31.2	512.3	25.3	533.9	30.2
g4	0.65200	6.79	0.08218	6.98	0.982	0.05754	1.32	509.1	34.2	509.7	27.2	512.3	29.4
g3	0.66570	6.36	0.08361	6.32	0.992	0.05775	0.81	517.6	31.5	518.1	25.8	520.3	18.2
g8	0.67050	5.95	0.08482	6.29	0.960	0.05733	1.76	524.8	31.7	521.0	24.3	504.3	39.0
g6	0.68890	6.38	0.08636	6.68	0.964	0.05785	1.78	534.0	34.2	532.1	26.4	524.1	39.3
g2	0.70510	7.17	0.08736	7.28	0.988	0.05853	1.13	539.9	37.7	541.8	30.1	549.7	25.1
g1	0.71110	7.09	0.08945	7.30	0.986	0.05766	1.23	552.3	38.6	545.4	29.9	516.9	27.5
Weighted Mean = 522 ± 23 [4.5%] 95% conf.; MSWD = 0.24													
TO 46, Band-e Hezar Chah, NE central Iran													
g6	0.71810	4.30	0.08920	4.38	0.982	0.05839	0.83	550.8	23.1	549.5	18.3	544.4	18.8
g3	0.75280	4.93	0.09393	4.91	0.976	0.05813	1.07	578.7	27.2	569.8	21.5	534.7	23.9
g1	0.76010	4.84	0.09470	4.89	0.986	0.05821	0.81	583.3	27.3	574.1	21.2	537.7	18.3
g2	0.75800	4.67	0.09492	4.80	0.985	0.05792	0.83	584.6	26.9	572.9	20.4	526.7	18.8
g5	0.77540	4.69	0.09630	4.72	0.993	0.05839	0.54	592.7	26.7	582.9	20.8	544.4	12.7
g4	0.79190	4.70	0.09824	4.73	0.990	0.05846	0.66	604.1	27.2	592.2	21.1	547.0	15.2
Weighted Mean = 581 ± 21 [3.6%] 95% conf.; MSWD = 0.53													
TO 50, Band-e Hezar Chah, NE central Iran													
g3	0.77620	4.61	0.09532	4.78	0.962	0.05906	1.31	586.9	26.8	583.3	20.5	569.3	29.0
g6	0.75190	4.67	0.09572	4.90	0.960	0.05697	1.37	589.3	27.6	569.3	20.4	490.4	30.5
g5	0.76930	4.84	0.09694	4.92	0.986	0.05756	0.81	596.5	28.1	579.4	21.4	513.1	18.4
g1	0.78720	4.69	0.09814	4.76	0.982	0.05817	0.90	603.5	27.4	589.6	21.0	536.2	20.2
g4	0.80630	4.70	0.09994	4.69	0.994	0.05851	0.52	614.1	27.5	600.4	21.3	548.9	12.2
g2	0.81770	5.06	0.10140	5.15	0.988	0.05848	0.79	622.6	30.6	606.8	23.1	547.8	17.8
Weighted Mean = 601 ± 22 [3.7%] 95% conf.; MSWD = 0.24													
TO-He4, Band-e Hezar Chah, NE central Iran													
g5	0.64610	4.01	0.08415	4.40	0.928	0.05569	1.64	520.8	22.0	506.1	16.0	440.0	36.8
g6	0.73780	4.61	0.09248	5.16	0.906	0.05786	2.19	570.2	28.1	561.1	19.9	524.5	48.2
g1	0.77410	4.96	0.09500	5.37	0.925	0.05910	2.04	585.0	30.0	582.1	22.0	570.8	44.6
g3	0.77800	4.84	0.09587	4.89	0.974	0.05886	1.11	590.2	27.6	584.3	21.5	561.9	24.7
g2	0.75620	4.74	0.09676	4.87	0.976	0.05668	1.06	595.4	27.7	571.8	20.7	479.1	23.8
g4	0.77800	4.81	0.09782	4.82	0.988	0.05768	0.75	601.6	27.7	584.3	21.4	517.6	17.2
Weighted Mean = 527 ± 35 [6.2%] 95% conf.; MSWD = 1.6													
LJ6, Lahijan, northern west Alborz mountains (Lam, 2002)													
g3/10	0.70480	2.48	0.08892	2.00	0.866	0.05748	1.25	549.1	10.5	541.6	10.4	510.2	27.4
g3/16s1	0.68010	3.41	0.08557	2.12	0.744	0.05764	2.31	529.3	10.8	526.8	14.0	516.2	50.8
g3/16s2	0.66840	2.70	0.08526	2.04	0.841	0.05686	1.48	527.4	10.3	519.8	11.0	486.2	32.7
g2/2	0.74190	2.01	0.09256	1.94	0.967	0.05813	0.51	570.7	10.6	563.5	8.7	534.8	11.2
g2/3	0.73520	2.26	0.09172	1.91	0.915	0.05813	0.93	565.7	10.4	559.6	9.7	534.7	20.3
g3/3	0.71520	4.33	0.09042	2.05	0.577	0.05737	3.57	558.0	11.0	547.8	18.3	505.6	78.5
g2/13	0.75540	3.46	0.09380	3.37	0.880	0.05840	1.67	578.0	18.6	571.3	15.1	544.9	36.6
g2/12	0.70020	2.98	0.08690	1.94	0.791	0.05843	1.87	537.2	10.0	538.9	12.4	546.1	40.8
g2/11	0.69880	2.25	0.08805	1.96	0.887	0.05756	1.04	544.0	10.2	538.1	9.4	513.1	22.9
g3/15	0.67730	4.34	0.08751	2.02	0.633	0.05613	3.44	540.8	10.5	525.1	17.8	457.6	76.2
g2/15	0.72580	2.20	0.09003	1.85	0.919	0.05847	0.88	555.7	9.9	554.1	9.4	547.3	19.3
g3/14	0.72170	2.32	0.08979	1.91	0.860	0.05830	1.19	554.3	10.2	551.7	9.9	540.9	25.9
g3/7	0.74170	2.51	0.09289	1.96	0.841	0.05791	1.37	572.6	10.7	563.4	10.9	526.3	30.0
g3/6	0.72360	3.04	0.08972	2.05	0.815	0.05850	1.82	553.9	10.9	552.8	13.0	548.4	39.7
Weighted Mean = 551 ± 9 [1.6%] 95% conf.; MSWD = 1.9													

Table 3
TIMS Zircon U-Pb Data

Fractions	Weight (mg)	U (ppm)	Pb* (ppm)	206 Pb‡ 204 Pb	Radiogenic ratios						% err	Ages			Corr. coef.†	Pb_c¥ (pg)	Pb*/ Pb_c
					208* Pb 206* Pb	206* Pb 238 U	% err	207* Pb 235 U	% err	207* Pb 206* Pb		206 Pb 238 U	207 Pb 235 U	207 Pb 206 Pb			
ZJ-2																	
Zircon 1	0.0401	4.43	0.86	412.3	0.424	0.15052	1.36	1.56826	1.72	0.07556	1.00	903.9	957.7	1083.5	0.8167	6.1	5.7
Zircon 2–4	0.0138	13.80	0.11	32.2	0.125	0.00822	11.00	0.09425	13.40	0.08318	8.52	52.8	91.5	1273.4	0.7734	9.4	0.2
Zircon 5 & 6	0.0310	32.17	0.01	35.0	0.133	0.00044	32.80	0.00163	65.10	0.02709	51.20	2.81	1.65	−1484.5	0.6306	3.7	0.1
Zircon 7–13	0.0426	11.60	0.35	19.6	0.191	0.00043	110.00	0.01171	73.10	0.19720	90.60	2.78	11.82	2803.2	0.5730	1.0	15.1
Zircon 14–17	0.0609	70.19	0.03	34.1	0.151	0.00043	9.90	0.00320	15.20	0.05440	10.20	2.75	3.25	387.6	0.7485	9.6	0.2
Zircon 18–25	0.0294	87.89	0.25	70.5	0.120	0.00279	3.61	0.02414	4.74	0.06264	2.85	18.0	24.2	696.0	0.8000	10.9	0.7
Zircon 26–30	0.0361	52.79	0.04	33.5	0.159	0.00079	11.20	0.00157	111.00	0.01441	107.00	5.10	1.60	0.00	0.3833	8.5	0.2
Zircon 31–33	0.0323	50.21	0.02	36.6	0.252	0.00044	21.50	0.00362	29.40	0.06034	18.60	2.81	3.67	6.16	0.7771	4.5	0.2
Zircon 34	0.0500	54.77	0.03	38.2	0.221	0.00043	14.00	0.00211	43.40	0.03555	39.00	2.78	2.14	−665.2	0.4607	5.9	0.2
Zircon 35–38	0.0415	165.49	0.08	40.4	0.232	0.00044	7.02	0.00298	11.60	0.04875	7.99	2.86	3.02	135.6	0.7343	11.0	0.3
Zircon 39–49	0.0935	166.08	3.75	4294.2	0.194	0.02041	0.50	0.25631	0.51	0.09108	0.11	130.3	231.7	1448.2	0.9783	6.7	52.3
Zircon 50–52	0.0467	287.22	0.14	48.1	0.213	0.00044	4.60	0.00296	8.29	0.04855	6.01	2.85	3.00	126.3	0.7043	15.0	0.4
Zircon 53	0.0437	254.78	0.12	142.9	0.175	0.00043	5.46	0.00305	10.70	0.05135	8.65	2.78	3.09	256.4	0.5965	4.5	1.1
Zircon 54–61	0.1195	124.66	0.16	284.9	0.205	0.00116	1.67	0.00787	2.69	0.04925	2.00	7.46	7.96	159.9	0.6703	6.1	3.1
Zircon 62–68	0.0311	57.85	1.78	483.4	0.064	0.03108	0.71	0.36534	0.76	0.08525	0.25	197.3	316.2	1321.3	0.9422	9.2	6.0
Zircon 69–77	0.0505	83.01	0.07	44.3	0.255	0.00080	5.18	0.00475	11.30	0.04304	9.63	5.16	4.81	−165.3	0.5348	10.4	0.4
ZJ9																	
Zircon a	0.0066	307.82	25.64	10174.0	0.085	0.69355	0.50	0.08463	0.49	0.05944	0.11	523.7	534.9	583.2	0.9780	3.1	54.6
Zircon b	0.0096	341.74	28.60	19.1	0.091	0.68450	0.64	0.08466	0.62	0.05864	0.15	523.9	529.5	553.8	0.9710	11.2	24.5
Zircon c	0.0050	436.83	39.47	1872.8	0.109	0.72871	0.50	0.08999	0.49	0.05873	0.12	555.5	555.8	557.1	0.9700	8.6	22.9
Zircon d	0.0053	211.14	18.97	1405.8	0.140	0.70978	0.63	0.08710	0.58	0.05910	0.22	538.4	544.6	570.9	0.9380	6.4	15.7
Zircon e	0.0096	422.24	39.58	3177.9	0.108	0.76544	0.48	0.09332	0.47	0.05949	0.10	575.1	577.1	585.1	0.9780	9.4	40.4
ZJ11																	
Zircon a	0.0130	366.94	3.25	2368.3	0.192	0.05461	1.04	0.00829	0.88	0.04777	0.54	53	54	88	0.8500	3.1	13.6
Zircon b	0.0154	148.53	1.39	616.0	0.260	0.05438	2.08	0.00830	1.63	0.04753	1.22	53	54	76	0.8100	4.0	5.3
Zircon c	0.0181	210.02	1.82	418.7	0.164	0.05364	1.92	0.00830	1.07	0.04686	1.50	53	53	42	0.6200	7.0	4.7
Zircon d	0.0087	143.00	1.32	36.8	0.241	0.05919	11.20	0.00827	5.70	0.05191	8.49	53	58	282	0.6700	38.0	0.3
Zircon e	0.0141	199.06	1.84	438.8	0.229	0.05464	1.61	0.00842	1.31	0.04709	0.87	54	54	54	0.8400	5.6	4.6

Analytical data for granites from the Zanjan–Takab area, northwest Iran.

Note: Zircon dissolution followed the methods of Krogh (1973) and Parrish (1987). Elemental separation was done with a HBr anion column chemistry for lead and HCl column chemistry for uranium. Decay constants used were $^{238}U = 0.15513 \times 10^{-9}$ yr^{-1} and $^{235}U = 0.98485 \times 10^{-9}$ yr^{-1} (Steiger and Jager, 1977). Isotopic analyses were determined on a VG Sector multicollector thermal ionization mass spectrometer. A mass fractionation correction of 0.10%±0.05%/amu, as determined by standard runs on NBS 981 (common lead) and NBS 982 (equal atom lead), was applied to the lead data. Samples were spiked with a either a mixed $^{205}Pb/^{235}U$ spike or a mixed $^{208}Pb/^{235}U$ spike. Errors on $^{206}Pb/^{204}Pb$ were minimized by use of a Daly multiplier and are typically on the order of 1% or less. Errors for $^{206}Pb/^{204}Pb$ were reduced further on samples spiked with ^{205}Pb by using a dynamic Daly calibration after the technique of Roddick et al. (1987, p. 115). Common lead corrections were made using values determined from Stacey and Kramers (1975) for the interpreted crystallization age.

*Radiogenic component.

‡Ratios corrected for spike and mass fractionation only.

Numbers in parentheses are analytical errors in percent. For measured and radiogenic ratios this is the 2-sigma value for the ratio, e.g, 0.1750 (15) means 0.1750±0.0015. Errors were computed using data algorithm of Ludwig (1989).

†Corr. coef. is the correlation of $^{206}Pb/^{238}U$ and $^{207}Pb/^{2235}U$ errors as determined by Ludwig (1989).

¥Total amount of common Pb in analysis. Pb*/Pb_c is the ratio of radiogenic to common Pb in the analysis.

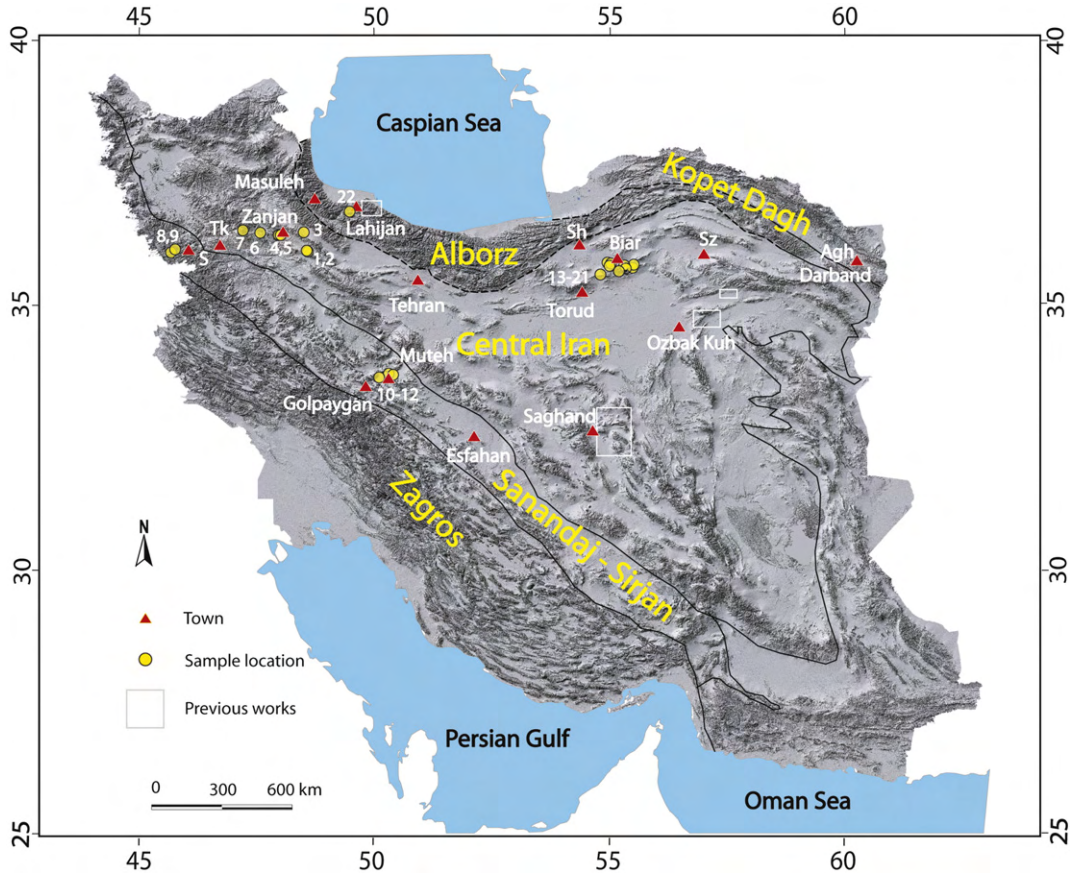

Fig. 1. Sample locations on SRTM image depicting topography, mountain belts and tectonic zones of Iran. Sample numbers follow sample order in Table 1. Town name abbreviations: Biar: Biarjmand, S: Saqqez, Sh: Shahrud, Sz: Sabzevar, Tk: Takab.

creating the supra-subduction Semail oceanic plate. They attribute the final oceanic closure prior to continent–continent collision due to the subduction of the remnant Semail plate. The suture lies in southern Iran between the Zagros and an accretionary arc complex (Sanandaj–Sirjan zone and Urumieh–Dokhtar arc) of central Iran (Fig. 1) (Berberian and King, 1981). Considerable discussion persists as to whether the collision is linked to deformation of Late Cretaceous, Paleogene, or late Miocene age (e.g., Berberian and King, 1981; Axen et al., 2001).

As shown on the location map (Fig. 1) studied samples are from various localities across central Iran and the Sanandaj–Sirjan structural zone. We discuss the results of our investigation starting in the Zanjan area, where the type locality of Precambrian granites of Iran is situated (Stöcklin and Setudehnia, 1970), and from there proceed counterclockwise to other occurrences, following the order presented in Table 1.

4. Analytical results and geological context

4.1. Northwest Iran

Stöcklin and Setudehnia (1970) proposed that the granites exposed in northwestern Iran represent the oldest Precambrian basement complex in all of Iran. The exposed crystalline basement can overall be subdivided into two types of rocks: sheared and foliated granitic orthogneisses and equigranular to porphyritic undeformed granites. In the following sections we will discuss the geological setting and the new U-Pb zircon ages derived for a suite of granites and granitic orthogneisses collected in the Soltanieh ranges south of Zanjan and west Zanjan-Takab highlands along the Qezel Ozan River, the largest drainage system of this region (Fig. 1).

4.1.1. Soltanieh Mountains

The Soltanieh Mountains are located along the southern margin of the Tarom Mountains (western Alborz) that are structurally controlled by SW-vergent Pliocene thrust faults along their southern margin, thrusting crystalline basement and metasediment over Oligo-Miocene and younger sedimentary strata. The Soltanieh Mountains are mainly underlain by Late Proterozoic to Jurassic strata that are intruded by the following three major granitic plutons: (1) Sarv-e Jahan granite, (2) Khoram Darreh granite, and (3) Doran granite.

4.1.1.1. Sarv-e Jahan granite. A 7 by 2 km outcrop area consisting mostly of foliated granite represents the easternmost example of Neoproterozoic plutons in the Soltanieh Mountains (Alavi-Naini, 1994). The granite clearly intrudes the Late Proterozoic Kahar Formation (with Rb-Sr model age of 645 Ma, Crawford, 1977) and is cut by several thin hornblende lamprophyre dikes of unknown age. Zircons separated from

two different rock types in Sarv-e Jahan granite (Fig. 2) have yielded concordant ion-microprobe U-Pb ages (Table 2). A sample of the deformed granite ZJ4, representing the dominant lithology in the area, gave a weighted mean $^{206}Pb/^{238}U$ age of 544±29 Ma with MSWD=1.9 (n=8) (Fig. 2B). Sample ZJ3, a medium grained leucocratic granite, yielded very small zircons from which three relatively larger grains were individually analyzed and yielded a weighted mean $^{206}Pb/^{238}U$ age of 599±42 Ma with MSWD=0.015 (n=3) (Fig. 2A).

4.1.1.2. Khorram Darreh granite. The Khorram Darreh granite occupies a low-lying area of the central portion of the Soltanieh Mountains west of the city of Soltanieh (Table 1). It is predominantly composed of a voluminous equigranular biotite granite with several slightly more mafic subdomains along the northern margin of the pluton. The irregular, roughly 10 by 6 km granite intrudes the Neoproterozoic Kahar Formation and shales of the Jurassic Shemshak formation. A sample from the main equigranular biotite granite (sample ZJ11) was used to constrain

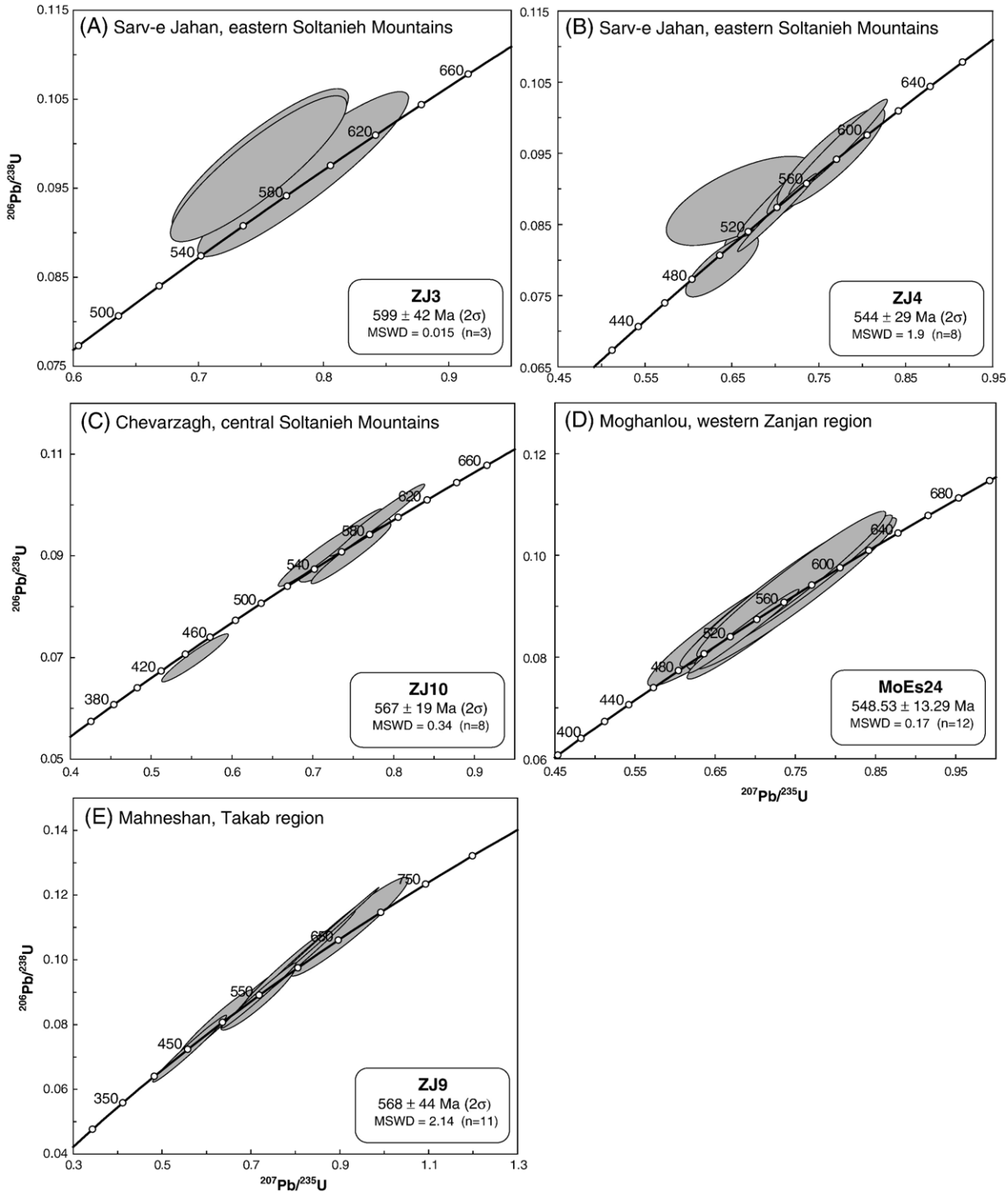

Fig. 2. Concordia diagram showing ion microprobe zircon U-Pb data from the Soltanieh mountains and Takab area in NW Iran. See text for discussion.

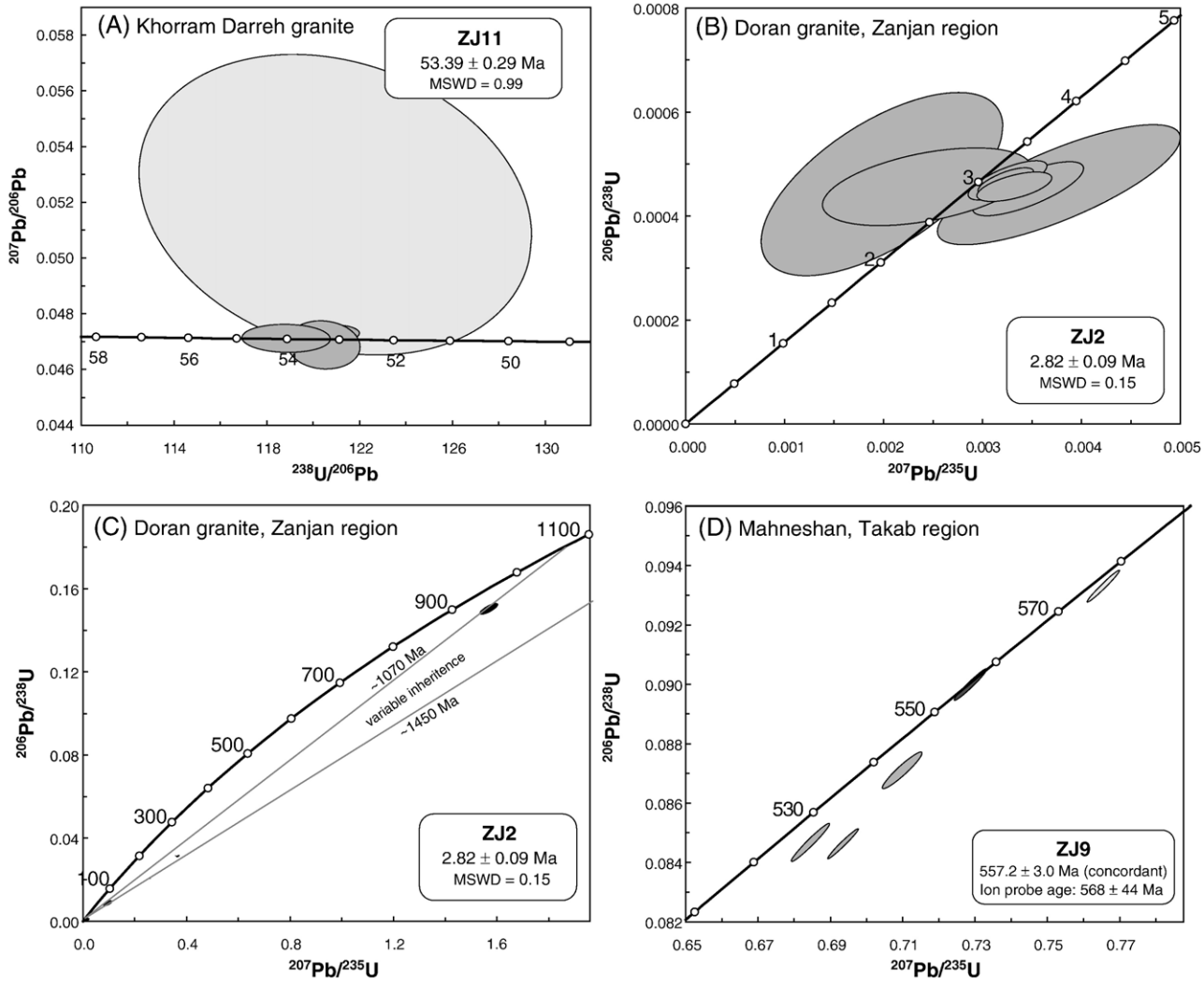

Fig. 3. Concordia diagrams showing TIMS zircon U-Pb data (Table 3). (A) Khorram Darreh Eocene granite in the central Soltanieh Mountains. (B) Concordant zircon U-Pb ages interpreted to be the crystallization age of sample ZJ2 from Doran leucrogranite. See Fig. 4 for location. (C) Discordant zircon U-Pb analyses characterized by inherited cores, indicating a Mesoproterozoic inherited zircon component either from a magmatic or detrital source. (D) Sample ZJ9 from a granitic orthogneiss west of Mahneshan see Fig. 6 for location. Discordant TIMS analyses show complex zircon inheritance and Pb loss, while the single concordant analysis is within error of ion-microprobe age.

the intrusion age of this discordant granite body (Table 3). TIMS zircon U-Pb age data on five multigrain (2–4) and single grain aliquots yielded a concordant mean age of 53.4±0.4 Ma with MSWD=1.13 (n=5) (Fig. 3A). This Eocene intrusion age is similar to reported widespread Cretaceous to Eocene intrusion ages within the Alborz Mountains and the Urumieh–Dokhtar magmatic arc; magmatism that is related to northward subduction of the Neotethys prior to continental collision in the Zagros.

4.1.1.3. Doran granite. A small body of deeply eroded leucogranite is partially exposed in the low topography around the village of Doran, about 12 km south of Zanjan. Stöcklin et al. (1965) and Stöcklin and Eftekharnezhad (1969) mapped this body as the "Doran granite" (Figs. 1 and 4). Furthermore, they asserted that the siliciclastic Neoproterozoic Bayandor Formation unconformably overlies the eroded and saprolitic surface of the granite along its northern contact. Based on this relationship, the "Doran granite" has been established in the literature as the type example of Precambrian plutonism in Iran. Early isotopic dating attempts of the "Doran granite" and its presumed equivalents using whole-rock Rb-Sr systematics failed to yield meaningful results (Crawford, 1977). The same study also reported a biotite Rb-Sr age of 175±5 Ma which should be interpreted as the cooling age of the granite below ~300 °C (McDougall and Harrison, 1999).

The dominant rock type at Doran is a severely crushed snow-white leucogranite (almost entirely lacking mafic minerals) that is extensively quarried for feldspar directly southeast of the type locality where the disconformity between "Doran granite" and the Neoproterozoic sedimentary rocks was reported (Fig. 4). We refer to the leucogranite as the Doran leucogranite. Zircons from the Doran leucogranite (sample ZJ2) were dated by TIMS zircon U-Pb geochronology and yielded a concordant age of 2.8±0.1 Ma with MSWD=0.14 (n=8) (Table 3) (Fig. 3B). This astonishingly young age suggests that the main phase of the Doran leucogranite is not Precambrian, but

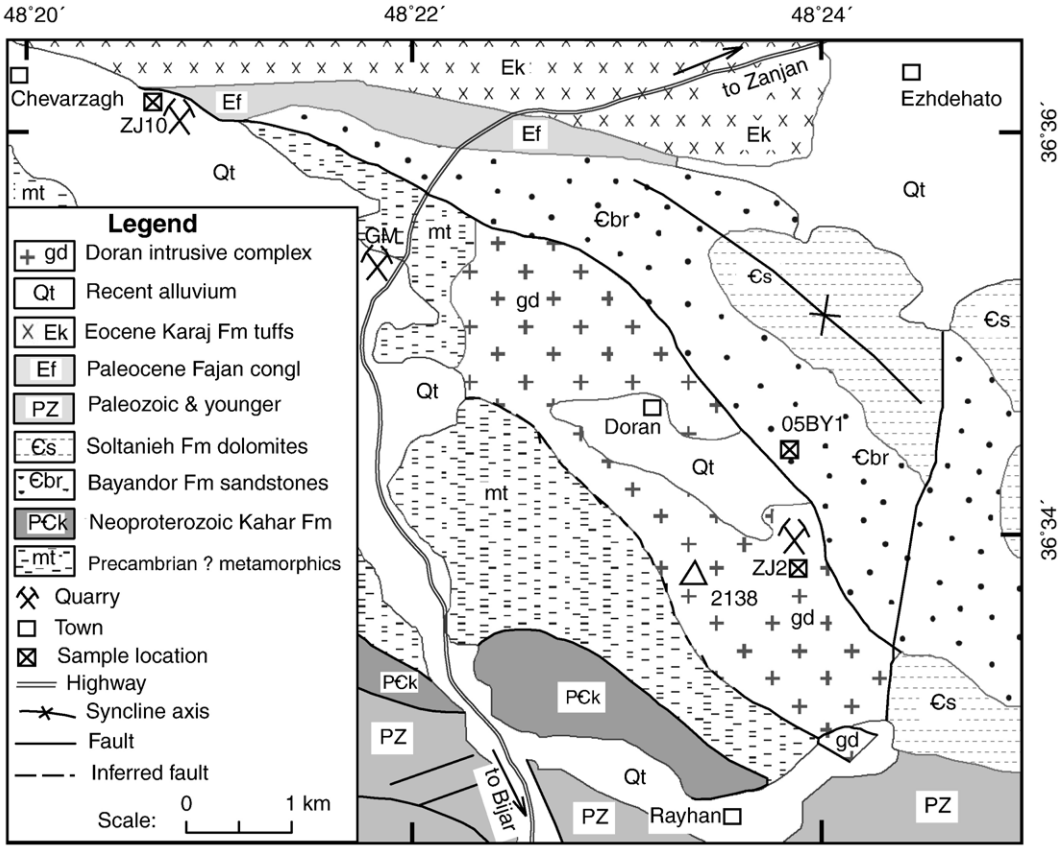

Fig. 4. Simplified geologic map of Doran granite modified after Stöcklin et al. (1965) and Babakhani and Sadeghi (2005). Recent excavations that have exposed granite in two locations (labeled ZJ10 and GM) west of Zanjan–Bijar road are added and indicate that the pluton extends west under Quaternary alluvium (Qt). Granite is faulted against Bayandor and Fajan Formations in its northern margin. Square labeled 05BY1 represents sample location near the type section of the Bayandor Formation used in detrital zircon study (Horton et al., 2008-this issue). Open triangle corresponds to the local summit where Doran leucogranite cuts Doran biotite granite. See text for discussion.

Pliocene. Several analyses ($n=8$) yielded significantly older Neo- and Mesoproterozoic discordant ages (Table 3) (Fig. 3C). Detailed cathodoluminescence imaging revealed the presence of inherited cores in some of the zircons yielding discordant ages. The discordant U-Pb analyses do not regress to a reasonable discordia, indicating that more than one inherited component must have been present in the analyzed zircons. More work is needed to resolve whether the inherited component is derived from a detrital or magmatic source. The presence of older detrital zircons with near-concordant U-Pb ages of ~1870 Ma in the siliclastic rocks of the Neoproterozoic Tashk Formation has been documented by Ramezani and Tucker (2003). These widely distributed rocks (correlative with the Kahar Formation in northern and western Iran) could be the source of old xenocrystic zircons in many of the magmatic rocks of the region. Alternatively, the inherited zircons might suggest the presence of a Mesoproterozoic magmatic source in the subsurface that is older than the widespread Neoproterozoic Peri-Gondwanan basement — an inherited component similar to that observed in non-juvenile basement rocks of the eastern Arabian Shield (Johnson and Woldehaimanot, 2003). In light of the absence of a 1000–1500 Ma detrital zircon population in Cambrian–Tertiary strata of central Iran (Horton et al., 2008-this issue) (Fig. 4), we currently favor a magmatic source for the inherited component.

It is worth mentioning that published geologic maps (Stöcklin et al., 1965, Stöcklin and Eftekharnezhad, 1969; Babakhani and Sadeghi, 2005) show the "Doran granite" as a single-phase granitic pluton confined to the region east of the Zanjan–Bijar highway. Approximately 0.5 km southwest of the quarry (sample ZJ2), however, small apophyses of the ~2.8 Ma Doran leucogranite sharply cut a more altered, pinkish and weakly foliated granite that contains partly altered biotites (Fig. 4). Zircons of the weakly foliated pinkish granites have yet to be dated, but our field observations imply that the dominant white leucogranite likely intrudes an older intrusion. We will refer to this older intrusion as the Doran biotite granite. Recent excavations by local miners have unearthed two small occurrences of granite west of the Zanjan–Bijar highway (Fig. 4). One is an intensely argillized granite briefly quarried for kaolinite just to the east of Chevarzagh village and ~4 km northwest of Doran (Fig. 4). Along its northern side, a fault juxtaposes the granite against the Paleocene Fajan conglomerate that is devoid of any granitic clasts. Sample ZJ10 (Table 1) represents this altered granite (Fig. 4). Eight individual ion-microprobe spot analyses on zircons from sample ZJ10 gave concordant U-Pb ages with a $^{206}Pb/^{238}U$ weighted mean age of 567±19 Ma and MSWD=0.34 ($n=8$) (Table 2) (Fig. 2C), which is statistically indistinguishable from the age of the foliated Sarv-e Jahan granite discussed earlier, and verifies the existence of Neoproterozoic plutonism at Doran.

Given the relationship between the Neoproterozoic biotite granite and the large Pliocene leucogranite body, we consider it likely that the biotite Rb-Sr age from a "Doran granite" of 175±5 Ma reported by Crawford (1977) pertains to the older pink biotite granite. It is also noteworthy that no Neoproterozoic cores were found in the ~2.8 Ma Doran leucogranite.

Stöcklin et al. (1965) proposed that the contact between the "Doran granite" and the overlying Neoproterozoic Bayandor Formation is an unconformity. However, the complex intrusive nature (Pliocene main body of the "Doran granite") and the faulted nature of the northern contact between the Neoproterozoic biotite granite and the Bayandor Formation (as well as the Fajan conglomerate) question this assumption. Horton et al. (2008-this issue) have suggested a depositional age ≤559±28 Ma (2σ uncertainty) based on detrital zircon U-Pb analyses from the basal portion of the Proterozoic Bayandor Formation (~0.5 km north of Doran) (Fig. 4). The ages of the Doran biotite granite and the Bayandor Formation are indistinguishable and the relative age relationship is therefore inconclusive in terms of resolving the nature of the contact. However, the fact that the basal Bayandor Formation contains no locally-derived basal conglomerate and the basal red shales and sandstones lack granitic clasts leads us to favor an intrusive or tectonic nature of the original contact between the Bayandor Formation and the Doran biotite granite. The so-called kaolinite layer that Stöcklin et al. (1964, 1965) interpreted as a saprolitic horizon below an unconformity is likely a fault gouge related to a shallowly-dipping fault. This observation appears to be supported by the structural juxtaposition of both Bayandor Formation and Fajan conglomerate against the granite across this fault east of Chevarzagh (Fig. 4). This fault appears to be Pliocene in age, as suggested by a newly excavated quarry just to the west of Zanjan–Bijar road that exhibits highly sheared Doran leucogranite (GM) in fault contact (Fig. 4).

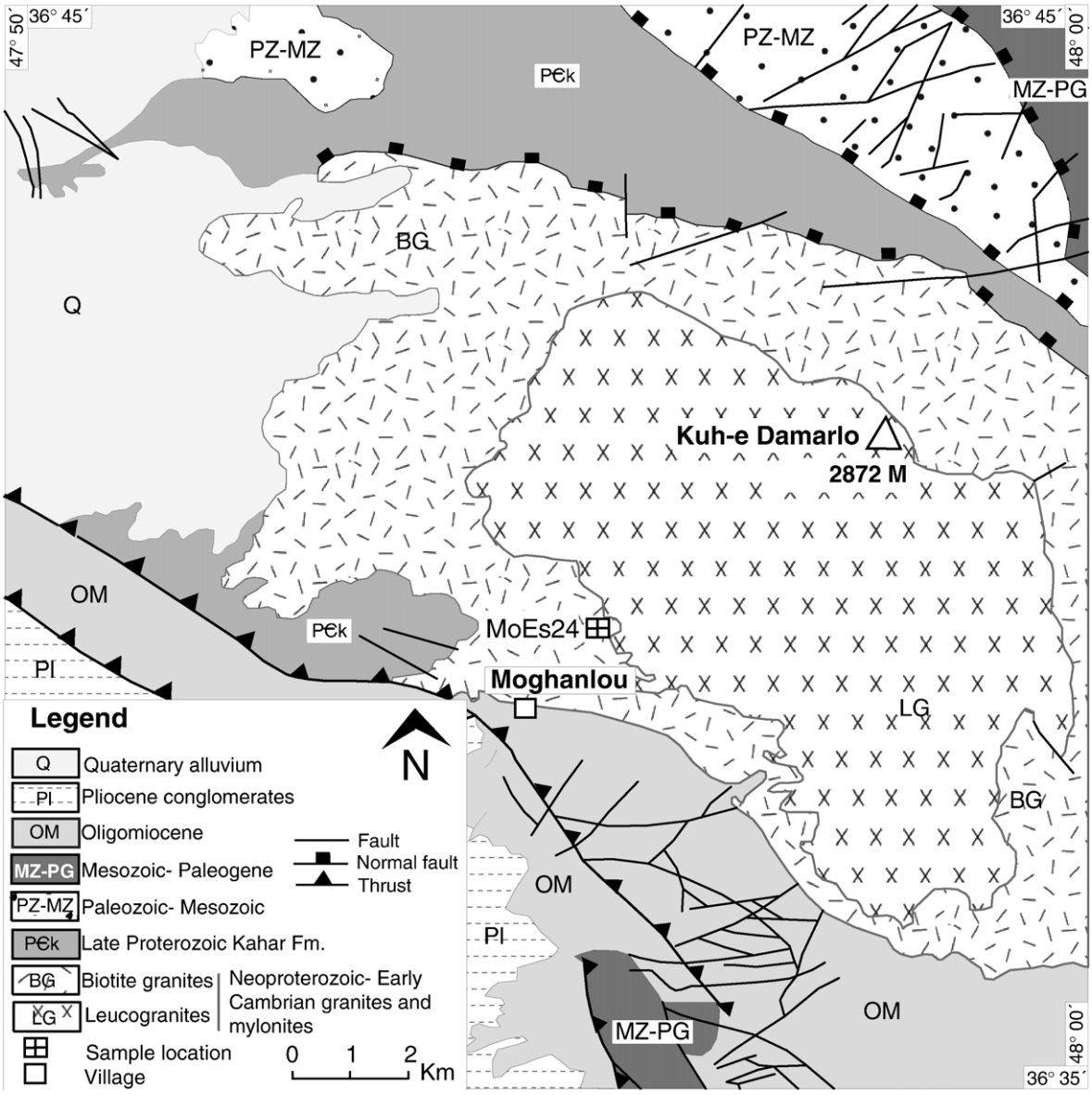

Fig. 5. Simplified geologic map of Moghanlou core complex, west Zanjan area, east of Qezel Ozan River (modified after Lotfi, 2001).

Our new zircon U-Pb data from the Doran area is of regional importance, since many presumed Precambrian granitoids in Iran, especially in northwestern Iran, are often referred to as "Doran-type" granites. Additional U-Pb zircon dating on various intrusive phases within the granite complex around Doran and Takab (see below) is necessary and currently in progress to further resolve these issues surrounding the age of the "Doran-type" granites.

4.1.2. Takab-west Zanjan area

At its western extension, the Soltanieh Mountains join the uplands bordering the Qezel Ozan River. Those uplands between the cities of Zanjan and Takab in western Iran contain a large crustal block made up of high-grade orthogneisses, granitic rocks, and Proterozoic to Cambrian sedimentary rocks. As we show below, Neoproterozoic plutonic rocks make up a large portion of this coherent crustal block (Fig. 1). The following two localities were studied: (1) Moghanlou area, and (2) Mahneshan area.

4.1.2.1. Moghanlou area. A large, dome-shaped and intensely sheared Neoproterozoic granitoid complex is exposed in the border zone of the Zanjan and Mahneshan geological maps (Babakhani and Sadeghi, 2005; Lotfi, 2001) to the east of Qezel Ozan River (Fig. 5). The pluton intrudes the Neoproterozoic siliciclastic rocks of the Kahar Formation and is composed of several different compositional phases. The body of the Moghanlou granite is a biotite-rich granitic orthogneiss (sample MoEs24) and is well exposed in the vicinity of an antimony mine, near Moghanlou village (Fig. 5). Twelve ion-microprobe spot analyses on five individual zircons of the Moghanlou granitic orthogneiss yielded concordant ages with weighted mean $^{206}Pb/^{238}U$ age of 548±27 Ma and MSWD=0.16 (n=12) (Table 2) (Fig. 2D).

According to maps of Zanjan and Mahneshan (Babakhani and Sadeghi, 2005; Lotfi, 2001), the dome of Neoproterozoic granites and their sheared equivalents, together with the Neoproterozoic country rocks in the footwall, are in fault contact with younger un-metamorphosed rock units of various ages — the youngest being the Miocene Upper Red Formation. Based on "younger-on-older" juxtaposition along this fault, we tentatively interpret that these NW trending dominant faults of this area are normal, suggesting a possible metamorphic core complex exhumed in the Miocene time (Fig. 5). A similar relationship has been documented in Mahneshan area, where Stockli et al. (2004) documented the presence of two low-angle normal faults juxtaposing Neoproterozoic basement and Oligo-Miocene red beds.

4.1.2.2. Mahneshan area. Directly across the Qezel Ozan River west of Moghanlou a large, biotite-rich, porphyritic, granite orthogneiss is exposed to the southwest of the town of

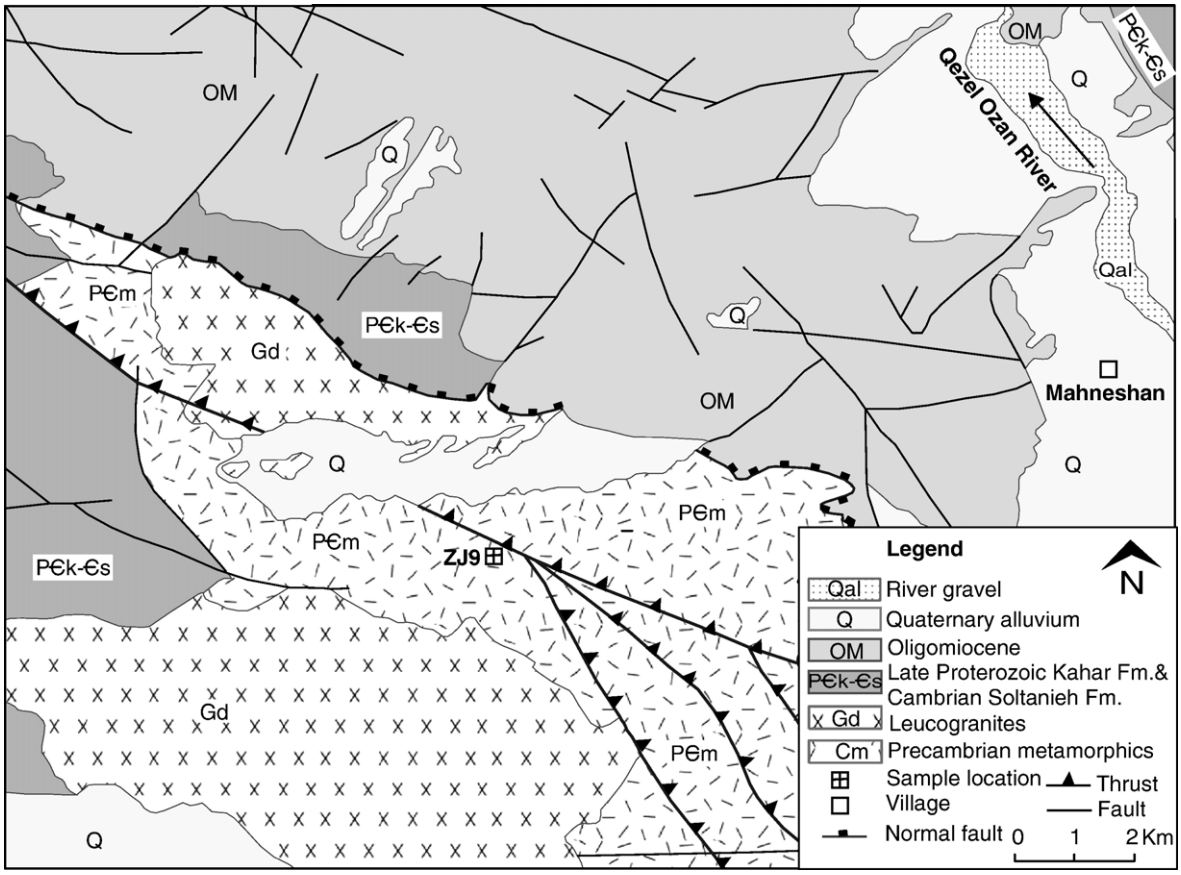

Fig. 6. Simplified geologic map of Mahneshan area, west of Qezel Ozan River. Low-angle normal faults and Tertiary extensional exhumation of the basement rocks have been documented by Stockli et al. (2004). Map modified after Lotfi (2001).

Mahneshan (Fig. 6). This orthogneiss is characterized by a high-temperature deformation fabric with a vertical foliation (sample ZJ9). It occurs as a large body that is bound on the north and south sides by two north-dipping detachment faults of Tertiary age. Along the southern margin, the lower detachment juxtaposes it against an Oligocene granite (~25 Ma), formerly considered a Doran-type granite (Stockli et al., 2004). Eleven individual ion-microprobe U-Pb isotopic analyses on ten zircon grains from the orthogneiss sample ZJ9 yielded concordant U-Pb ages with weighted mean $^{206}Pb/^{238}U$ age of 568±44 Ma and MSWD=2.1 (n=11) (Table 2) (Fig. 2E). TIMS analyses on the same sample exhibited a more complicated record of variable inheritance and lead loss, yielding a best-estimate intrusion age of 557.2±3.0 Ma (Table 3) (Fig. 3D). Given the likelihood of variable inheritance and lead loss, we prefer the ion-microprobe age as the more reliable crystallization age.

Based on field reconnaissance and geo- and thermochronological studies, Stockli et al. (2004) argued for an important Oligo-Miocene intra-arc extensional event in this region that was subsequently overprinted by late Neogene, regionally widespread contraction caused by the continent–continent collision between the Arabian plate and Iranian crustal fragments. It is noteworthy that the world class non-sulfide Zn deposit at Anguran is located nearby within this coherent basement complex. This ore deposit was previously known as an example of Precambrian mineralization in Iran (e.g., Samani, 1988) until Gilg et al. (2006) attributed the mineralization to the above mentioned Miocene intra-arc extension and formation of a metamorphic core complex identified by Stockli et al. (2004).

4.2. Northwestern Sanandaj–Sirjan zone

In the northwestern part of the Sanandaj–Sirjan structural zone (Fig. 1), numerous granitoids are exposed within extensive realms of sheared lower greenschist-facies rocks with Precambrian protolith ages (e.g., Eftekhar-Nezhad, 1973). The shear

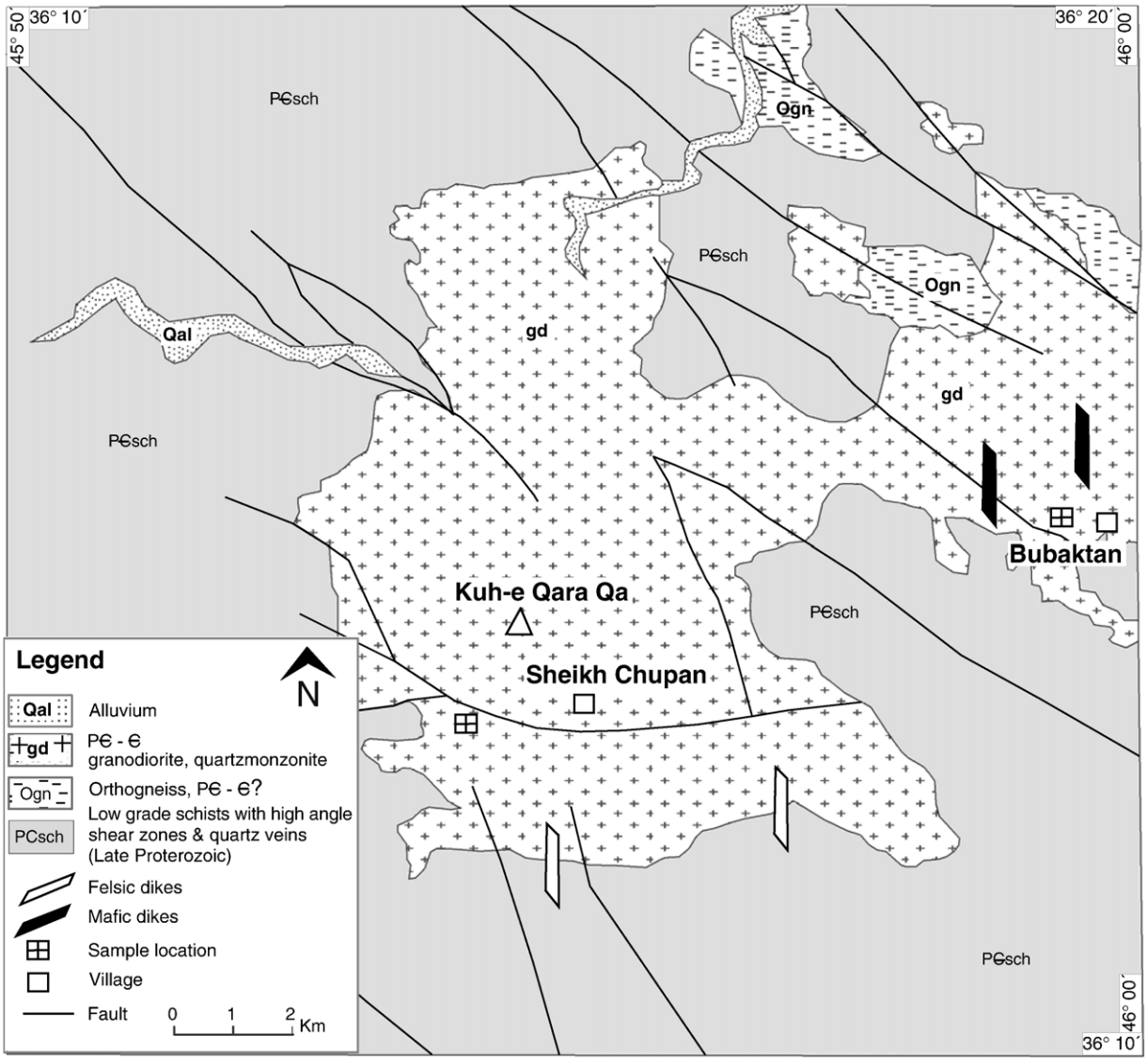

Fig. 7. Simplified geologic map of the Sheikh Chupan-Bubaktan sheared pluton and the surrounding regional low grade metamorphic rocks in Kurdestan Province of Iran (modified after Omrani and Khabbaznia, 2003).

zones bear indications of gold mineralization in several locations. The crystallization ages of these granitoids in the northwestern part of the Sanandaj–Sirjan, however, are disputed; while Eftekhar-Nezhad (1973) assigned the plutons to the so-called Doran-type granite (i.e., late Precambrian age), Omrani and Khabbaznia (2003) revised the age to post-Cretaceous. To resolve the debate, a large composite pluton to the west of the city of Saqqez was targeted in this study and two samples were collected at the Qara Qa mountain (Fig. 7) near the Iraqi border (Fig. 1).

The sample from the Sheikh Chupan side (Fig. 7) is a shallow biotite-hornblende granodiorite with abundant zoned plagioclase. Field observations indicate that the Sheikh Chupan granitoid does not intrude the sheared rocks and that it might represent the non-sheared equivalent of the greenschist protolith. Ion microprobe analyses on zircons from the Sheikh Chupan

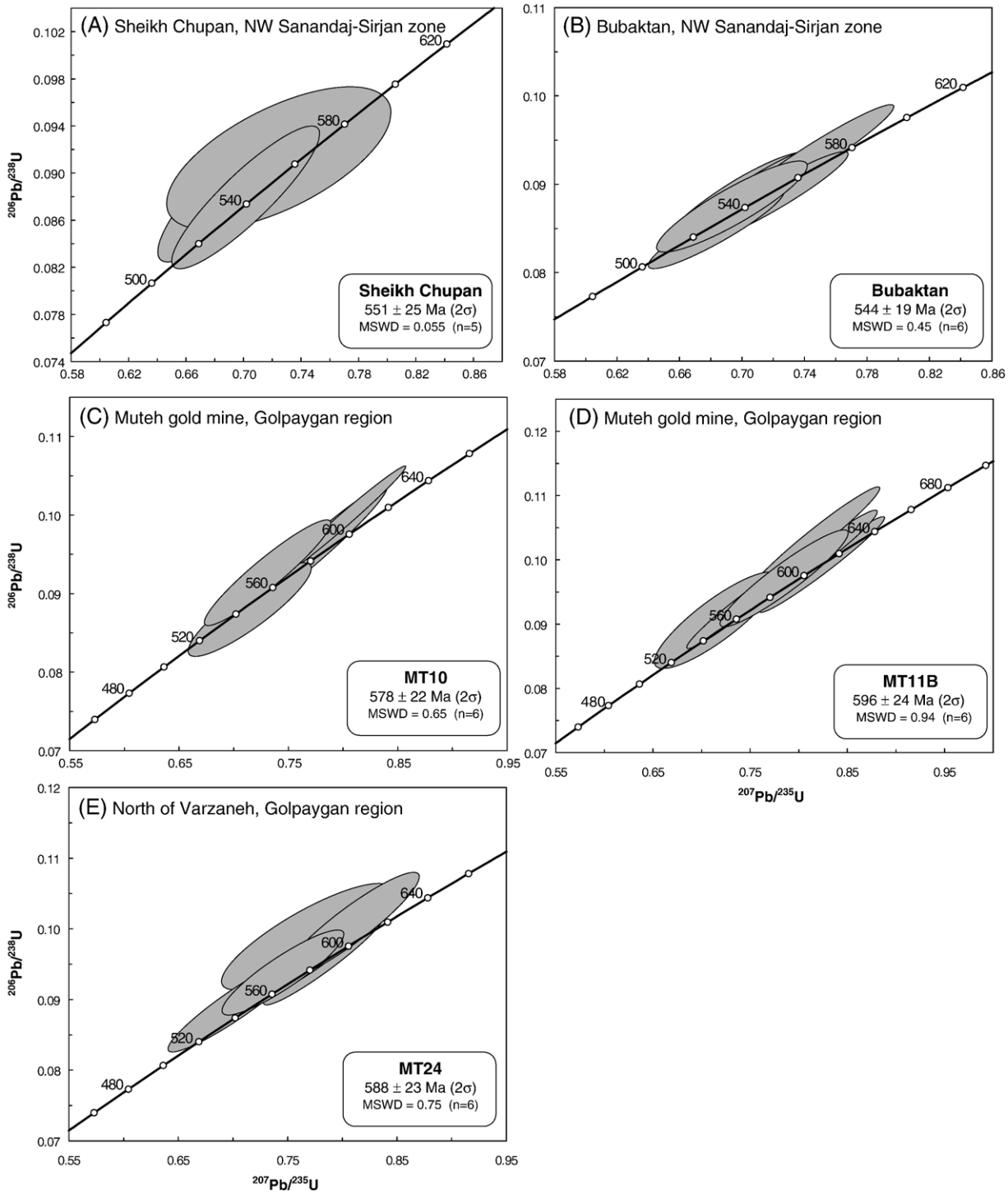

Fig. 8. Concordia diagrams showing ion-microprobe zircon U-Pb data for rocks from Sanandaj–Sirjan zone (Fig. 1).

granodiorite yielded concordant U-Pb ages with $^{206}Pb/^{238}U$ weighted mean age of 551±25 Ma and MSWD=0.055 (n=5) (Table 2) (Fig. 8A).

In contrast to the Sheikh Chupan granodiorite, the sample from Bubaktan farther east lacks hornblende and zoned plagioclase and is more deformed (Fig. 7). Zircons from the Bubaktan foliated biotite granite yielded concordant U-Pb ages with $^{206}Pb/^{238}U$ weighted mean age of 544±19 Ma, MSWD=0.45 (n=6) (Table 2) (Fig. 8B).

4.3. Golpaygan area

The Golpaygan area lies along the border zone between the Sanandaj–Sirjan zone and Urumieh–Dokhtar Tertiary magmatic arc in central Iran (Fig. 1) and was the study area for the first geologic map published by Geological Survey of Iran. Granitic rocks within the Golpaygan region were first discussed by Thiele et al. (1968) and reported to be "Doran-type" granites. This age assignment was contested by Rachidnejad-Omran et al. (2002), who suggested these grantitic rocks to be considerably younger in age. To shed light on this controversy, we collected two undeformed granites and one granitic orthogneiss from two subdomains of Golpaygan area, the Muteh gold mine region and the Varzaneh region (Fig. 9).

4.3.1. Muteh Au mine

The Muteh gold deposit occurs within a lower greenschist metamorphic complex of presumably Precambrian age approximately 50 km northeast of Golpaygan (Fig. 1). According to Thiele et al. (1968), the Muteh leucogranite intrudes Precambrian metamorphic rocks and appears to be older than the Neoproterozoic/Cambrian Soltanieh dolomite. Rachidnejad-Omran et al. (2002), however, considered younger ages for the meta-volcano-sedimentary host of Muteh granite, suggesting a Paleozoic protolith age and Mesozoic age for metamorphism. Based on their interpretation, one would expect the unmetamorphosed Muteh granite to be Mesozoic or Tertiary. Rachidnejad-Omran et al. (2002) reported the following K-Ar ages from the Muteh granite: 128.3±4.7 Ma and 124.4±4.4 Ma (whole rock), and 68.9±1.0 Ma and 67.5±1.0 Ma (biotite).

Our samples of the Muteh leucogranite were collected from the hills to the northwest of the Chah Khatoon open pit at the Muteh gold mine (Fig. 9) and are medium grained granites in intrusive contact with a dark gray to green hornfels (Table 1). Zircons separated from the Muteh leucogranite (sample MT10) gave concordant U-Pb ages with $^{206}Pb/^{238}U$ weighted mean age of 578±22 Ma, MSWD=0.65 (n=6) (Table 2) (Fig. 8C). Zircons separated from a biotite-rich variety of the granite

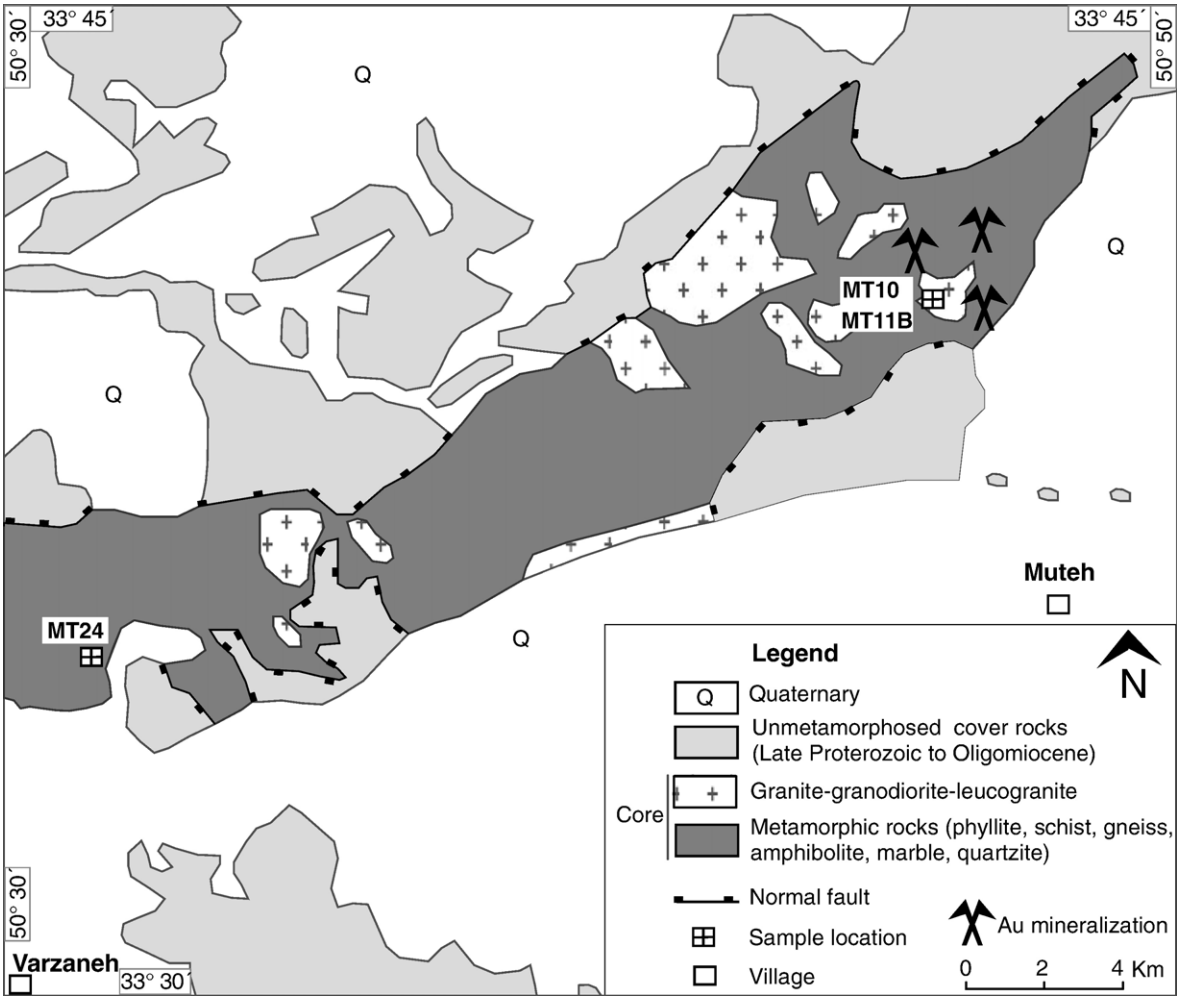

Fig. 9. Simplified geologic map of Muteh core complex, northwest of Esfahan, central Iran (modified after Thiele et al., 1968).

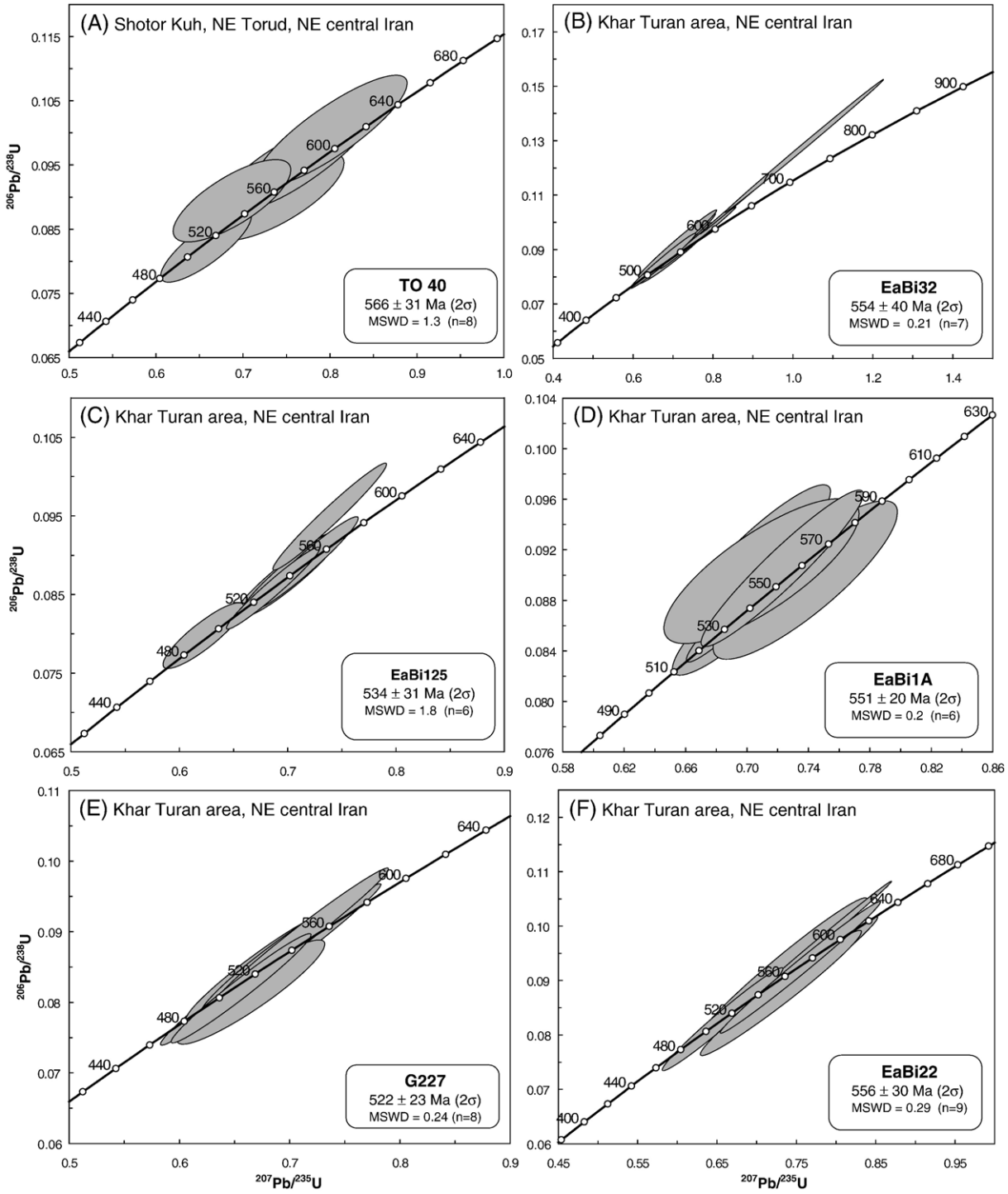

Fig. 10. Concordia diagrams showing ion-microprobe zircon U-Pb data for rocks from Torud and Khar Turan area, northeast central Iran (Fig. 1).

(sample MT11B) yielded somewhat older, but still concordant, U-Pb ages with $^{206}Pb/^{238}U$ weighted mean age of 596±24 Ma, MSWD=0.94 (n=6) (Table 2) (Fig. 8D). These new U-Pb zircon ages verify the existence of Neoproterozoic plutonic rocks in the Muteh area. A corollary of this result is that, unlike the postulation by Rachidnejad-Omran et al. (2002), the metamorphosed sedimentary rocks hosting the Muteh granite are not Paleozoic in age; rather, the Neoproterozoic Kahar Formation or its equivalents initially proposed by Thiele et al. (1968) are the likeliest choice for the metamorphosed country rock.

4.3.2. Varzaneh metamorphic rocks

A large dome of high grade metamorphic rocks is exposed in the Haji Qara mountains, north of the village of Varzaneh and about 25 km west of Muteh gold mine (Fig. 9). Part of the complex consists of biotite granite orthogneisses. Sample MT24 is a biotite- and quartz-rich variety and was collected to

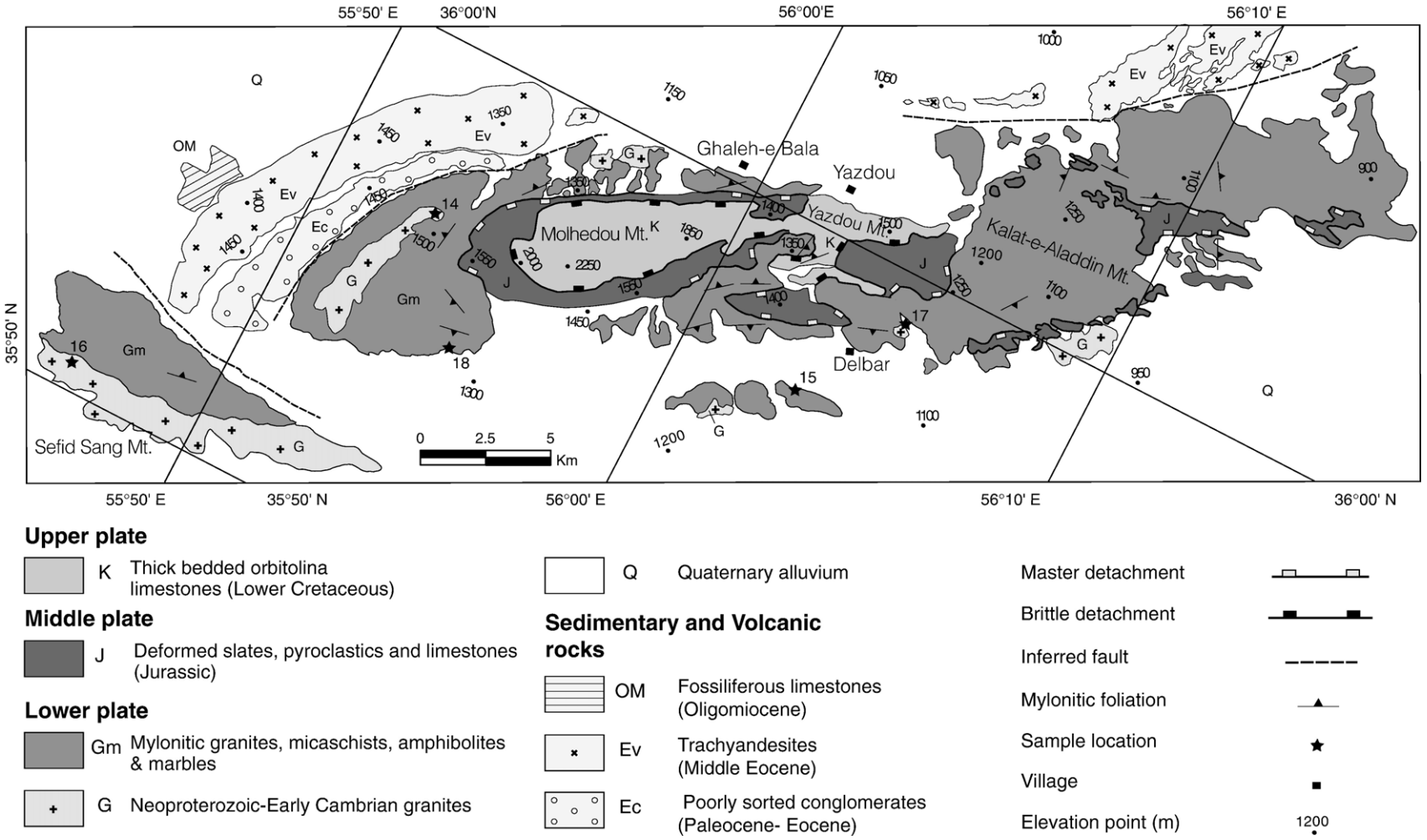

Fig. 11. Simplified geologic map of Khar Turan core complex between northeast central Iran and eastern Alborz (modified after Malekpour, 2005; Hassanzadeh et al., 2005).

investigate the protolith age of the gneiss for comparison with Muteh granites. Zircons separated from sample MT24 yielded concordant U-Pb ages with $^{206}Pb/^{238}U$ weighted mean age of 588±23 Ma, MSWD=0.59 (n=6) (Fig. 8E), indicating a Neoproterozoic protolith (Table 2) that is within error of the crystallization age of the Muteh granites.

A brief discussion of the timing of metamorphism, Au mineralization, and exhumation in north Golpaygan region is relevant here. Based on the Neoproterozoic protolith age of the MT24 granite orthogneiss, the metamorphic event(s) postdates Neoproterozoic. A K-Ar age of 174.5±2.9 Ma, that Rachidnejad-Omran et al. (2002) reported for a nearby amphibolite, clearly points to the peak of thermal recrystallization in Middle Jurassic time. Mica $^{40}Ar/^{39}Ar$ and K-Ar ages constrain the subsequent cooling path, with these rocks cooling below ~300 °C in Eocene times (Rachidnejad-Omran et al., 2002; Moritz et al., 2006). In light of detailed new $^{40}Ar/^{39}Ar$ ages, Au mineralization at Muteh, previously thought to be Precambrian (e.g., Samani, 1988), is now considered to be Eocene in age (Moritz et al., 2006). Tillman et al. (1981) have described the effects of an important post-Cretaceous extensional event on a large area between Golpaygan and Esfahan and Verdel et al. (2007) have postulated that the crystalline terrain north of the Golpaygan region could represent a metamorphic core complex (Fig. 9).

4.4. Northeast central Iran: Torud-Khār Turan-Band-e Hezar Chāh region

A large arid region of basin and range topography covering >5000 km^2 is located between the eastern Alborz and the Great Kavir (desert) depression of central Iran, exposing several large and small Neoproterozoic granite and orthogneiss bodies (Fig. 1).

4.4.1. Torud area

About 50 km northeast of the small desert town of Torud, a metamorphic complex containing abundant granite orthogneisses is exposed in the area of Shotor Kuh. Hushmandzadeh et al. (1978) assumed a Precambrian age for these metamorphic rocks and their map shows that the foliation appears to continuously wrap around the mountain of Shotor Kuh. Our field investigations have verified their findings and show that foliation radially dips away from the core of the complex, demonstrating a characteristic gneiss dome. Previous attempts by Crawford (1977) of Rb-Sr radiometric dating of these metamorphic rocks failed. We analyzed a biotite-rich granite gneiss with augen fabric from the northwestern side of Shotor Kuh (sample TO-40). Zircons separated from TO-40 yielded concordant U-Pb ages with $^{206}Pb/^{238}U$ weighted mean age of 566±31 Ma, MSWD=1.3 (n=8), indicating a Neoproterozoic protolith (Table 2) (Fig. 10A). Ilkhchi et al. (2006) have reported protolith crystallization age of these orthogneisses at ca. 520 Ma by laser ablation ICP-MS analysis of zircon.

4.4.2. Khār Turan area

In the mountains about 15 km SSW of the town of Biarjmand, a northeast-trending metamorphic complex is exposed (Fig. 11). The complex mainly consists of amphibolite-grade gneisses and schists that Navai (1987) considered to be Precambrian in age. Patches of less sheared granites can be found on various scales within gneisses and schists. These less deformed granitic lenses have previously been thought to be either post-Jurassic to pre-Cretaceous (Navai, 1987) or post-Cretaceous (Huber, 1977). To resolve these issues, we collected four different granites and one strongly deformed granite gneiss samples from Khar Turan.

Sample EaBi32 was collected at Kuh-e Sefid Sang (Fig. 11) and is a biotite-rich granite containing distinctive zoned allanites. Seven individual ion microprobe spot analyses on zircons yielded concordant ages with weighted mean $^{206}Pb/^{238}U$ age of 554±40 Ma with MSWD=0.21 (n=5) (Table 2) (Fig. 10B).

Zircons separated from a white leucocratic variety of the granite (sample EaBi125) yielded slightly younger concordant U-Pb ages with $^{206}Pb/^{238}U$ weighted mean age of 534±31 Ma, MSWD=1.8 (n=6) (Table 2) (Fig. 10C). Another sample of the white leucocratic variety of the granite (EaBi-1A) at the western tip of the complex, embedded in orthogneisses, yielded concordant U-Pb ages with $^{206}Pb/^{238}U$ weighted mean age of 551±20 Ma, MSWD=0.20 (n=6), indicating a Neoproterozoic protolith (Fig. 10D). A fine grained biotite-garnet granodiorite with zoned plagioclase (sample G227) yielded the youngest concordant U-Pb ages with $^{206}Pb/^{238}U$ weighted mean age of 522±23 Ma, MSWD=0.24 (n=8) (Fig. 10E).

These results clearly indicate that Kuh-e Sefid Sang granite and its associated intrusions were emplaced in the Neoproterozoic–Early Cambrian and do not belong to either the post-Jurassic to pre-Cretaceous or post-Cretaceous group of intrusions as speculated by Navai (1987) and Huber (1977), respectively.

Sample EaBi22 is a biotite-garnet mylonite and like the EaBi32 granite contains characteristic zoned allanites. Zircons separated from the EaBi22 gneiss yielded concordant U-Pb ages with $^{206}Pb/^{238}U$ weighted mean age of 556±30 Ma, MSWD=0.29 (n=9), indicating a Neoproterozoic protolith (Fig. 10F). Based on similar trace element patterns for allanites, Malekpour (2005) argued that the EaBi22 mylonite is derived from the shearing of EaBi32-type granite. Our U-Pb results support such a hypothesis by revealing statistically similar crystallization ages for those rocks.

These new U-Pb ages clearly illustrate that the Biarjmand complex is cored by Neoproterozoic granites (Fig. 11). This core of the Biarjmand complex is structurally overlain by: (1) a lower greenschist-grade carapace of Jurassic volcaniclastic rocks and calcareous slates with a mylonitic fabric and (2) an unmetamorphosed cliff-forming cover section exposed at Kuh-e Molhedou consisting of Jurassic–Cretaceous carbonates, exhibiting only brittle deformation (Fig. 11). The core and the two overlying structural units are separated by two major low-angle faults suggestive of a metamorphic core complex (Malekpour, 2005). Recent thermochronologic investigations have revealed slow Mesozoic cooling from ~550 to 180 °C until ~70 Ma followed by abrupt rapid cooling (Hassanzadeh et al., 2005).

4.4.3. Band-e Hezar Chāh

Band-e Hezar Chāh is an area to the south of the city of Shahrud (Fig. 1) and in contrast to the other two sub-domains of

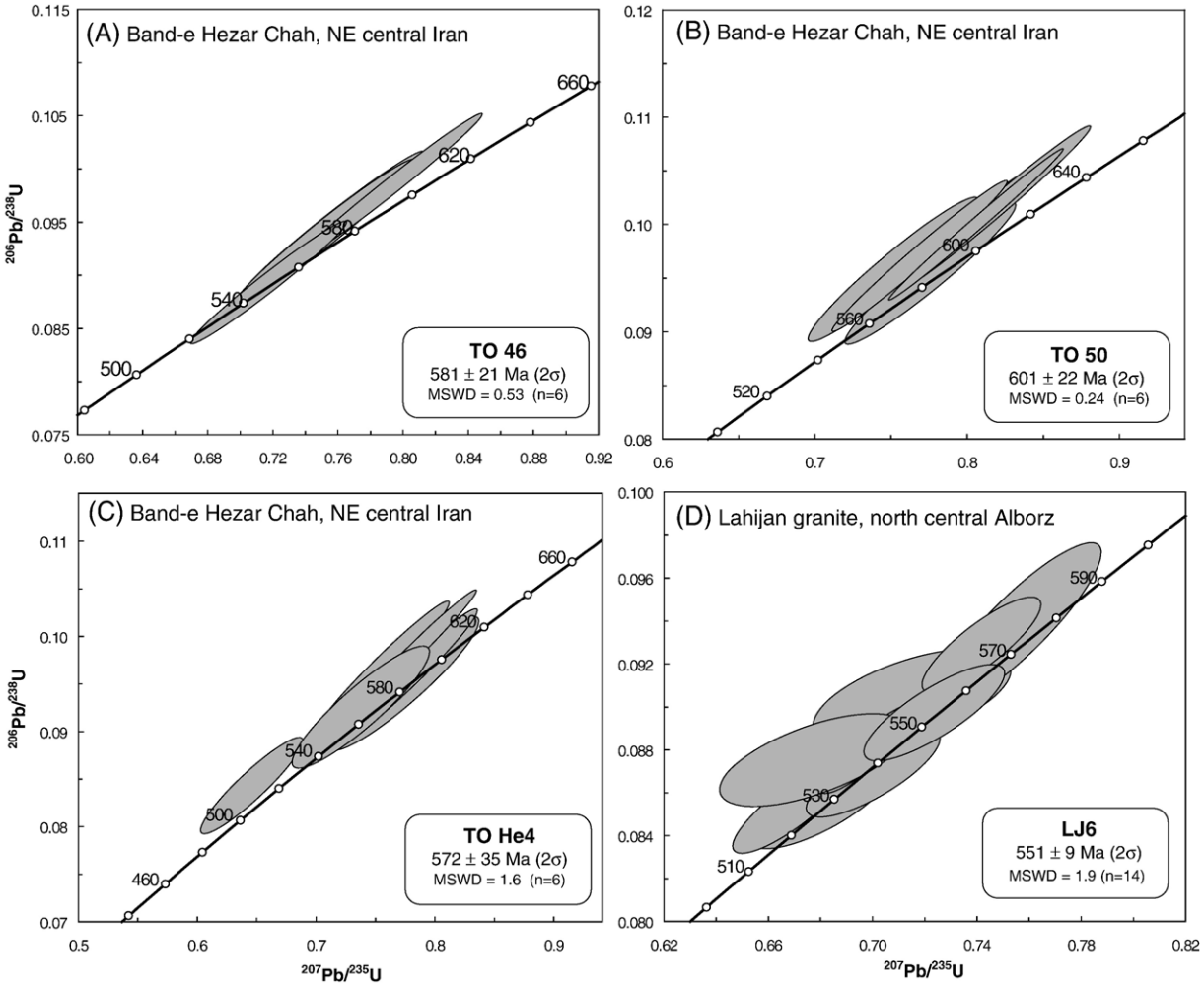

Fig. 12. Concordia diagrams showing ion-microprobe zircon U-Pb data for rocks from the Band-e Hezar Chāh area to the south of the city of Shahrud, and Lahijan pluton in the northwestern Alborz mountains (Fig. 1).

northeast central Iran (Torud and Khār Turan), is characterized by rolling hill topography with countless outcrops of Neoproterozoic granites and related metamorphic rocks in between Mesozoic sedimentary rocks. Sample TO-46 is from a slightly foliated, pink, medium grained large granite body that is in sheared contact with surrounding orthogneisses. Six individual ion microprobe analyses on zircons from sample TO-46 have yielded concordant U-Pb ages with weighted mean $^{206}Pb/^{238}U$ age of 581±21 Ma, MSWD=0.53 (n=6) (Table 2) (Fig. 12A).

Sample TO-50 is from the surrounding granite orthogneisses adjoining TO-46. Six individual ion microprobe analyses were also performed on zircons from sample TO-50 and yielded concordant U-Pb ages with weighted mean $^{206}Pb/^{238}U$ age of 601±22 Ma, MSWD=0.24 (n=6) (Table 2) (Fig. 12B).

Sample TO-He4 is a rounded gray orthogneiss cobble from a monolithologic conglomerate within a thick overlying package of Jurassic conglomerates, sandstones, and shales. Plant fossils (Genus *Klukia Raciborsky*, Genus *Coniopteris Brongniart*, Genus *Cladophlebis Brongniart*, cf. Genus *Labifolia Rasskazova et Lebedev*) obtained from a shale unit a few meters above the sampled monolithologic conglomerates indicate a middle Jurassic age (pers. comm. M. Sadegh Fakhr, 2006). Six of the zircons separated from this sample were individually analyzed by ion-probe and gave concordant U-Pb ages with weighted mean $^{206}Pb/^{238}U$ age of 572±35 Ma, MSWD=1.6 (n=6) (Table 2) (Fig. 12C). Although age equivalent with conglomerates of the Jurassic Shemshak Formation, the sampled conglomerate does not contain any Variscan-age granitic clasts derived from Eurasia or more typical Silurian–Devonian lydites derived from the Paleotethys suture zone. The origin of the monolithologic conglomerate, therefore, is likely related to middle Jurassic rifting, leading to the opening of major back-arc basins behind the arc of the now northward subducting Neotethys (Stampfli, 2000).

The occurrence of the conglomerate exclusively containing orthogneiss cobbles indicates rapid exhumation, potentially related to rifting, in Early Jurassic times and potentially makes the Band-e Hezar Chāh block's exhumation history quite distinct from the previously discussed Biarjmand complex in the Khār Turan block to the southeast.

4.5. Northern Alborz, Lahijan granite

Data for the Lahijan granite from northern Alborz along the shores of the Caspian Sea east of the city of Rasht (Fig. 1) is

integrated in this study after Lam (2002). According to Annells et al. (1975), the pluton intrudes presumably Carboniferous phyllitic metasedimentary rocks and clasts of the same granite occur in nearby Jurassic conglomerates; hence, a Triassic age was originally assigned to the granite (e.g., Berberian and Berberian, 1981). However, zircons separated from sample LJ6 yielded concordant U-Pb ages with $^{206}Pb/^{238}U$ weighted mean age of 551±9 Ma, MSWD=1.9 (n=14) (Fig. 12D), indicating a Neoproterozoic Peri-Gondwanan origin (Table 2). The Neoproterozoic crystallization age for Lahijan granite has major consequences. In terms of local geology, this age indicates that, unlike the previous interpretation by Annells et al. (1975), the contact with any possible Carboniferous metasedimentary rocks are not intrusive. The abundance of cataclastic zones supports a fault nature of the contact or subsequent strain localization along an originally intrusive contact.

More importantly, however, the occurrence of the Neoproterozoic Lahijan granite at the northern edge of the Alborz Mountains has profound implications for paleogeographic and plate tectonic reconstructions. The Lahijan granite seems to unequivocally indicate that the Alborz are underlain by basement with Gondwanan affiliation, precluding a Paleotethys in the Alborz as previously proposed by Stöcklin (1974).

4.6. Synopsis of published data

The following section presents a brief summary of published geochronologic work on Neoproterozoic granitoids of Iran. The earliest modern zircon U-Pb data include those of Samani et al. (1994) for the Saghand (east central Iran) and Ozbak Kuh (northern Lut block) areas (Fig. 1). Their U-Pb ages are mostly discordant and were interpreted to indicate magmatic and metasomatic events from middle to late Proterozoic.

Ramezani and Tucker (2003) and Verdel et al. (2007) present TIMS zircon U-Pb results from both multi-grain and single-grain zircon fractions for a range of rock units in the Saghand area of east central Iran (Fig. 1). Their zircon U-Pb data show that the Boneh–Shurow metamorphic complex is the oldest rock unit yielding an average Neoproterozoic–Cambrian $^{207}Pb/^{206}Pb$ age of 543±36 Ma; while some grains yielded older ages indicative of an inherited component typical for non-juvenile granitic melts or detrital inheritance. For a quartz-diorite said to intrude the Boneh–Shurow complex, concordant analyses were obtained with an average $^{207}Pb/^{206}Pb$ age of 547±3 Ma. For the well-known Zarigan-type leucogranites and granodiorites, commonly viewed as rough equivalents of the Doran granite, an average $^{207}Pb/^{206}Pb$ age of 533±8 Ma was obtained, with an older inherited component.

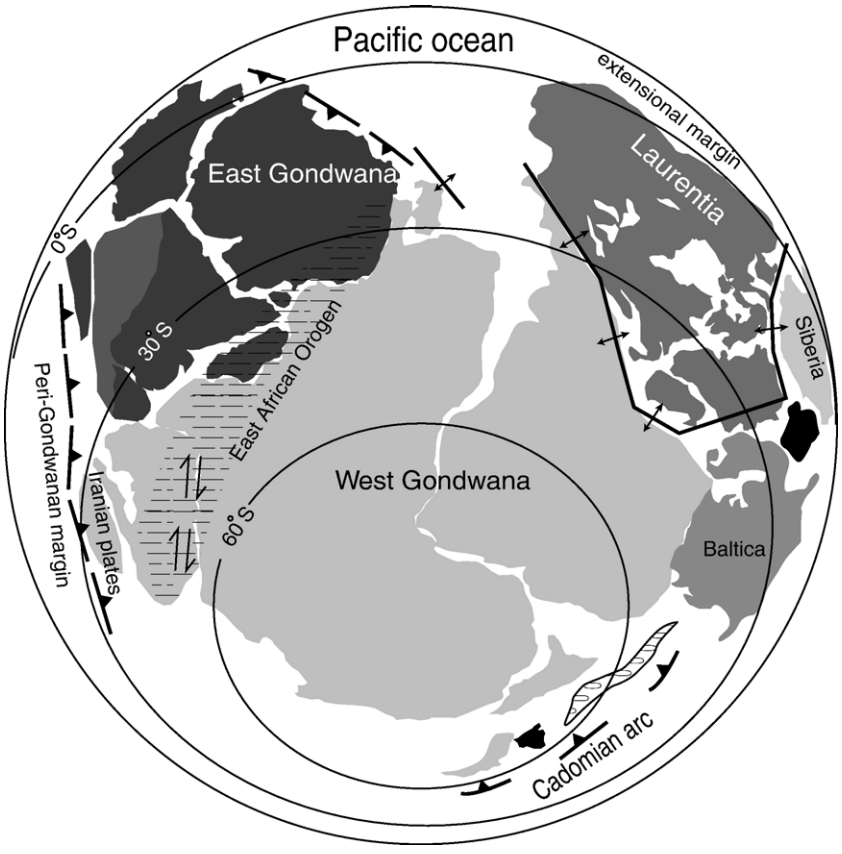

Fig. 13. Paleogeographic reconstruction at ~545 Ma after the amalgamation of eastern and western Gondwana (modified after Dalziel, 1997). In this time period, deformation within the northern portion of the East African Orogen (hatched pattern) postdates the main collisional tectonism and is dominated by post-orogenic dextral transcurrent deformation and extension. New U-Pb geochronology and integration with geological data show that Iranian continental blocks were situated in an Andean-style arc setting along the margin of Gondwana in what has been referred to as a peri-Gondwanan position.

5. Discussion

5.1. Paleogeography and plate tectonics

It is well accepted that crustal growth on Earth has not only been episodic but also regionally partitioned (e.g., Patchett and Chase, 2002). This perception allows certain age groups of rocks to be used as excellent paleogeographic indicators. A good example pertinent to this study is the prominent gap from ~900–500 Ma in the Laurentia crustal growth curve and abundance of ~900–500 Ma rocks in Arabian–Nubian Shield and adjoining regions of juvenile Gondwana (Veevers, 2003). Part of this time frame from ~900 to ~600 Ma, known as the Pan-African orogenic event, encompassed one of the broadest orogenies in Earth history (Mallard and Rogers, 1997; Rogers et al., 1995) and resulted in the final assembly of Gondwana, accompanied by immense emplacements of syn- and post-tectonic granites (Veevers, 2003; Johnson and Woldehaimanot, 2003).

Results of this study and other recent investigations discussed above demonstrate that late Neoproterozoic to Early Cambrian granitoids and granitic gneisses are present in all continental structural zones of Iran north of the Zagros, from the Sanandaj–Sirjan zone to the northern margin of the Alborz Mountains. Therefore, the crystalline basement of Iran can be considered to be the approximate northern continuation of the Arabian platform. This assertion excludes the Kopet Dagh Mountains in extreme northeastern Iran that constitute part of the Turan (i.e. Eurasian) basement poorly exposed near Agh Darband (Fig. 1) (Ruttner, 1993). Since definitive crust of comparable age is generally absent in cratonic Eurasia (e.g., Veevers, 2003), the occurrences of granitoids with Neoproterozoic ages from the Zagros to the northern foothills of the Alborz point to a Gondwanan affinity for the continental terranes composing Iran. It is noteworthy that not all of the above mentioned blocks of Iran have been explicitly grouped with Gondwana in previous paleogeographic reconstructions. For example, in considering Gondwanan fragments of Iran, Stern (1994) only mentions those of "western Iran".

Most Neoproterozoic paleogeographic reconstructions place the Iranian terranes along the Paleotethyan margin of Gondwana between the Zagros margin of Arabia and the northwestern margin of the Indian plate (e.g., Stampfli and Borel, 2004). The closest Pan-African belt to Iran is the East African Orogen which encompasses Proterozoic arc terranes of the Arabian–Nubian Shield. The main phase of convergent-margin magmatic activity along the Peri-Gondwanan margin of Iran (~550–530 Ma) coincided with strike-slip faulting and crustal extension within the East African Orogen (~640–550 Ma) (e.g., Stern, 1994) and clearly post-dated the main episode of the continental collision. In addition, the early Paleozoic platform sedimentation record of the Iranian region does not support a continental-collision magmatic scenario.

Therefore, based on the new age information and the tectonic setting of the Neoproterozoic rocks, we conclude that the Iranian blocks were originally part of a series of Peri-Gondwanan terranes, similar to the Avalonia (640–540 Ma) and Cadomia (616–540 Ma) arc terranes, occupying the northern margins of intact Gondwana (e.g., Murphy et al., 2004). These Peri-Gondwanan terranes were located long the active continental (Andean-style) margin of Gondwana and not part of the Pan-African belts associated with ocean closure and continent-continent collision (Fig. 13). Following Neoproterozoic-Early Cambrian intrusive activity, the Gondwanan blocks of Iran were separated from the Arabian–Nubian Shield and joined with Eurasia by sequential opening and closing of Paleotethys and Neotethys oceans.

The discovery of a Neoproterozoic–Early Cambrian granite along the northern foothills of the Alborz Mountains (Lam, 2002; Guest et al., 2006) questions the hypothesized position of Paleotethys suture in northern Iran south of the Lahijan area. The data support the notion that the suture does not continuously run along the northern flank of the Alborz mountains, south of the Caspian Sea (e.g., Sengör, 1990). The Paleotethys suture in the northwestern Alborz Mountains was originally envisaged by Stöcklin (1974) to exist in the Masuleh region about 100 km west of the Lahijan granite. Such conjecture implies that the metamorphic rocks in the Masuleh region should be of Varsican rather than Gondwanan origin (Davoudzadeh, 1997). Future investigations of the granite crystallization ages within the metamorphic complexes around Masuleh are needed to settle this critical debate and to shed further light on the position of Paleotethys suture in the South Caspian realm.

5.2. Basement composition and tectonic setting

From the initial descriptions of presumed Precambrian granitoids (e.g., Stöcklin and Setudehnia, 1970), a general misconception has arisen that the crystalline basement of Iran is dominantly leucocratic. Neoproterozoic rocks dated in this study display a wide range of compositions (including granites, granodiorites, and tonalites) and are commonly rich in biotite and in some cases contain significant percentages of hornblende (Table 1). Ramezani and Tucker (2003) also have documented the existence of Early Cambrian biotite-hornblende granodiorites in central Iran.

High alkalinity is also a quality that has been previously attributed to the Iranian basement granites (Berberian and Berberian, 1981, Lotfi, 2001, Omrani and Khabbaznia, 2003). However, the characteristic mineral phases of alkali granites, such as alkali pyroxenes and amphiboles, are entirely absent in these rocks. Thus, these granites should be named "alkali feldspar granite" rather than "alkali granite" to avoid a misleading referral to a rift-related setting. In fact, Ramezani and Tucker (2003) have strongly argued for a continental arc setting for the juvenile late Neoproterozoic–Early Cambrian granites of the Saghand region. Although an exotic origin for the Saghand granites has been proposed (Bagheri and Stampfli, 2008-this issue), the regional extent of similar age granites (this study) supports an active arc developed on Iranian crust in a Peri-Gondwanan setting.

5.3. Exhumation of Neoproterozoic–Early Cambrian basement

Neoproterozoic Peri-Gondwanan magmatism in Iran was followed by deposition of several kilometers of Paleozoic and

Mesozoic sedimentary and volcanic strata. It is, therefore, worthwhile to consider the mechanisms and timing of exhumation of the exposed Neoproterozoic–Early Cambrian granites and orthogneisses investigated in this study. Within the Zagros collision zone, the basement is entirely concealed beneath 8–12 km of passive-margin sedimentary rocks of the Arabian platform, with the exception of small basement fragments brought up in the Hormuz salt diapirs (Stöcklin and Setudehnia, 1970). No significant crystalline basement has been exhumed within the external or internal portions of the Zagros fold and thrust belt, although basement involvement has been postulated (e.g., McQuarrie, 2004).

Extensive exposures of granitic and metamorphic basement rocks are scattered throughout the remainder of central and northern Iran (Fig. 1). Based on field observations and a review of available stratigraphic and structural literature, the earliest significant basement exhumation occurred during Early to Middle Jurassic back-arc extension. Structurally, exhumed domal basement complexes containing Neoproterozoic–Early Cambrian granites and mylonites (e.g., northeastern central Iran, Muteh, Takab-west Zanjan and Saghand) are characterized by low-angle faults, juxtaposing this crystalline basement against younger, low-grade metamorphic or non-metamorphic rocks. Similar types of gneiss domes are integral components of metamorphic core complexes (e.g., Davis and Lister, 1988) and could be interpreted as shear zones at mid-crustal levels that were extensionally exhumed in Jurassic to Tertiary times (e.g., Hassanzadeh et al., 2005, Stockli et al., 2004; Verdel et al., 2007).

5.4. Neoproterozoic–Early Cambrian basement and ore deposits in Iran

Many Zn-Pb, Au and Fe-P ore deposits have traditionally been considered to have formed in Iran during the Precambrian (e.g., Samani, 1988). This inference was solely based on spatial association of ore bodies with presumed ancient rocks. However, recent radiometric dating suggests Tertiary mineralization ages for the enormous Zn deposit at Anguran (Gilg et al., 2006) and the modest Au deposit at Muteh (Moritz et al., 2006) discussed in this paper. Timing of epigenetic Au mineralization associated with the extensive shear zones in the Neoproterozoic–Early Cambrian basement of Kurdestan Province (northwestern Sanandaj–Sirjan zone) discussed earlier in this paper, remains unconstrained. Nevertheless, iron oxide-apatite ore deposits in the greater Saghand area (Fig. 1) are indeed related to Cambrian magmatic and metasomatic events (Samani, 1988; Samani et al., 1994; Ramezani, pers. comm.) based on isotopic age determinations. In summary, the aforementioned mineralizations in Iran can no longer be assumed to be Precambrian. Modern investigations have shown that the formation of major ore deposits in Iran is related to different distinct tectonic events spanning from the Precambrian to the Tertiary.

6. Conclusions

This study reveals that late Neoproterozoic to Early Cambrian granitoids and granitic gneisses are present in all structural zones of Iran north of the Zagros, from the Sanandaj–Sirjan zone to central Iran and the northern margin of the Alborz Mountains. Since granites of this age range are ubiquitous in the Gondwanan realm (including the Arabian-Nubian Shield) but absent in Laurentia, we conclude that most crystalline basement of Iran (excluding the Kopet Dagh structural zone) was part of Gondwana at that time. An active Peri-Gondwanan continental margin best explains the distribution of these granitoids in Iran.

Occurrence of the Neoproterozoic–Early Cambrian Lahijan granite south of the Caspian challenges the assumed position of Paleotethys suture in northern Iran south of the Lahijan area. Our data support the concept that the suture does not continuously run south of the Caspian Sea and show the need for a modern geochronological investigation of the complex crustal collage of northern Iran.

In contrast with the original descriptions of the Precambrian (i.e. Doran-type) granitoids of Iran, this work demonstrates that these rocks are neither typically leucocratic nor alkaline. Biotite-rich varieties are common in most cases and some granitoids contain hornblende. Typical mineral phases of alkali granites, such as alkali pyroxenes and amphiboles, are non-existent; therefore, use of the term “alkali” for these granites should not be used to avoid misleading referral to a rift-related setting.

The fact that Precambrian basement is concealed in the Zagros but is extensively exposed in the remainder of Iran may suggest that mechanisms other than thrust tectonics have been responsible for exhumation of the rocks investigated in this study. Extensional unroofing of Jurassic to Tertiary age is suggested for several cases. Understanding the tectonic history of individual cases of the late Neoproterozoic to Early Cambrian granitoids and granitic gneisses will require integrated, more detailed structural structural, petrological, and geochronological investigations.

Acknowledgements

This research was supported by Research Council of University of Tehran awarded to Hassanzadeh and National Science Foundation (grant EAR-0337775 to Horton and Axen) and (grant EAR-9902932 to Axen). We thank Dr. Mohammad Sadegh Fakhr for identifying plant fossils, Roghieh Akbar Ashrafi, Safia Omidian, Ahmad Reza Malekpour and Morteza Pirooz for help with figures, and David Gingrich, Jesse Mosolf, and Terrence Dewane for assistance with ion-microprobe and TIMS analyses. Extensive comments by reviewers Jahandar Ramezani and Gerard Stampfli, and editors Ezat Heydari and Rasoul Sorkhabi contributed greatly to the improvement of this text. The ion microprobe facility at UCLA is partly supported by a grant from the Instrumentation and Facilities Program, Division of Earth Sciences, National Science Foundation.

References

Alavi-Naini, M., 1994. Geological map of Khodabandeh-Soltanieh (scale 1:100,000). Geological Survey of Iran, Tehran, Iran.

Alavi, M., Vaziri, H., Seyed-Emami, K., Lasemi, Y., 1997. The Triassic and associated rocks of the Nakhlak and Aghdarband areas in central and

northeastern Iran as remnants of the southern Turanian active continental margin. Geological Society of America Bulletin 109, 1563–1575.

Annells, R.N., Arthurton, R.S., Bazely, R.A., Davies, R.G., 1975. Explanatory text of the Qazvin-Rasht quadrangles maps E3 and E4. Geological Survey of Iran, Tehran, Iran.

Axen, G.J., Lam, P.J., Grove, M., Stockli, D.F., Hassanzadeh, J., 2001. Exhumation of the west-central Alborz Mountains, Iran, Caspian subsidence, and collision-related tectonics. Geology 29, 559–562.

Babakhani, A.R., Sadeghi, A., 2005. Geological map of Zanjan (scale 1:100,000). Geological Survey of Iran, Tehran, Iran.

Bagheri, S., Stampfli, G.M., 2008. A new litho-structural subdivision for the Palaeotethys terranes in central Iran (Anarak, Jandaq and Posht-e-Badam areas) and its geodynamic implications. Tectonophysics 451, 123–155 (this issue). doi:10.1016/j.tecto.2007.11.047.

Berberian, F., Berberian, M., 1981. Tectono-plutonic episodes in Iran. In: Gupta, H.K., Delany, F.M. (Eds.), Zagros-Hindu Kush-Himalaya Geodynamic Evolution. Geodynamics Series, vol. 3. American Geophysical Union, Washington, D.C., pp. 5–32.

Berberian, M., King, G.C.P., 1981. Towards a paleogeography and tectonic evolution of Iran. Canadian Journal of Earth Sciences 18 (2), 210–265.

Compston, W., Williams, I.S., Meyer, C., 1984. U-Pb geochronology of zircons from lunar breccia 73217 using a sensitive high mass-resolution ion microprobe. Journal of Geophysical Research 89, 525–534.

Crawford, A.R., 1977. A summary of isotopic age data for Iran, Pakistan and India. Memoire hors serie n◦8. Societe geologique de France, pp. 251–260.

Dalziel, I.W.D., 1997. Neoproterozoic–Paleozoic geography and tectonics: review, hypothesis, environmental speculation. Geological Society of America Bulletin 108, 16–42.

Davoudzadeh, M., 1997. Iran. In: Moores, E.M., Fairbridge, R.W. (Eds.), Encyclopedia of European and Asian regional geology. Chapman and Hall, London, pp. 384–405.

Davis, G.A., Lister, G.S., 1988. Detachment faulting in continental extension; perspectives from the southwestern U.S. Cordillera. In: Clark, S.P., Burchfiel, B.C., Suppe, J. (Eds.), Processes in continental lithospheric deformation. Special Paper, vol. 218. Geological Society of America, pp. 133–159.

Dercourt, J., Zonenshain, L.P., Ricou, L.-E., Kazmin, V.G., Le Pichon, X., Knipper, A.L., Grandjacquet, C., Sbortschikov, I.M., Geyssant, J., Lepvreir, C., Perchersky, D.H., Boulin, J., Sibuet, J.-C., Savostin, L.A., Sorokhtin, O., Westphal, M., Bazhenov, M.L., Lauer, J.P., Biju-Duval, B., 1986. Geological evolution of the Tethys belt from the Atlantic to the Pamirs since the Lias. Tectonophysics 123, 241–315.

Eftekhar-Nezhad, J. 1973. The Mahabad Quadrangle map (scale 1:250,000). Geological Survey of Iran. Tehran, Iran.

Faure, G., Mensing, T.M., 2005. Isotopes, principles and applications. John Wiley & Sons, Inc., New Jersey.

Ghavidel-Syooki, M., 1995. Palynostratigraphy and paleogeography of a Paleozoic sequence in the Hassanakdar area, central Alborz range, northern Iran. Review of Palaeobotany and Palynology 86, 91–109.

Gilg, H.A., Boni, M., Balassone, G., Allen, C.R., Banks, D., Moore, F., 2006. Marble-hosted sulfide ores in the Anguran Zn-(Pb-Ag) deposit, NW Iran: Interaction of sedimentary brines with a metamorphic core complex. Mineralium Deposita 41, 1–16.

Guest, B., Stockli, D.F., Grove, M., Axen, G.J., Lam, P.S., Hassanzadeh, J., 2006. Thermal histories from the central Alborz Mountains, northern Iran: implications for the spatial and temporal distribution of deformation in northern Iran. Geological Society of America Bulletin 118, 1507–1521.

Haghipour, A., 1981. Precambrian in central Iran: lithostratigraphy, structural history and petrology. Iranian Petroleum Institute Bulletin 81, 1–17.

Hassanzadeh, J., Malekpour, A., Grove, M., Axen, G., Horton, B., Stockli, D.F., Farley, K., Schmitt, A., Mohajjel, M., Ghazi, A.M., 2005. Biarjmand metamorphic core complex: New evidence for Late Cretaceous–Paleocene extensional tectonics along the northern margin of central Iranian plateau. Geological Society of America Annual Abstracts with Programs 37 (7), 71.

Horton, B.K., Hassanzadeh, J., Stockli, D.F., Axen, G.J., Gillis, R.J., Guest, B., Amini, A.H., Fakhari, M., Zamanzadeh, S.M., Grove, M., 2008. Detrital zircon provenance of Neoproterozoic to Cenozoic deposits in Iran: Implications for chronostratigraphy and collisional tectonics. Tectonophysics 451, 97–122 (this issue). doi:10.1016/j.tecto.2007.11.063.

Huber, H., 1977. Geological map of Iran (scale 1:1000,000), sheet no. 2, north central Iran. National Iranian Oil Company, Tehran, Iran.

Hushmandzadeh, A., Alavi-Naini, M., Haghipour, A., 1978. Geological evolution of Torud area (Precambrian to recent). Geological Survey of Iran, Tehran, Iran. (in Farsi, with English abstract).

Johnson, P.R., Woldehaimanot, B., 2003. Development of the Arabian–Nubian shield: perspectives on accretion and deformation in the northern East African orogen and the assembly of Gondwana. In: Yoshida, M., Windley, B.F., Dasgupta, S. (Eds.), Proterozoic East Gondwana: Supercontinent Assembly and Breakup, vol. 206. Geological Society of London Special Publication, London, pp. 289–325.

Krogh, T.E., 1973. A low contamination method for hydrothermal decomposition of zircon and extraction of U and Pb for isotopic age determinations. Geochimica et Cosmochimica Acta 37, 485–494.

Krogh, T.E., 1982. Improved accuracy of U-Pb ages by the creation of more concordant systems using an air abrasion technique. Geochimica et Cosmochimica Acta 46, 637–649.

Ilkhchi, M.R., Faryad, S.W., Schulmann, K., Kosler, J., 2006. Metamorphism and exhumation processes of the Shotur Kuh metamorphic complex, Semnan Province (Central Iran Zone). Geolines abstract 20, p. 55.

Lam, P.J., 2002. Geology, geochronology, and thermochronology of the Alam Kuh area, central Alborz Mountains, northern Iran. M.S. thesis, University of California, Los Angeles, 135 p.

Lotfi, M., 2001. Geological map of Mah Neshan (scale 1:100,000). Geological Survey of Iran, Tehran, Iran.

Ludwig, K.R., 1989. Pb-Dat: A computer program for processing raw Pb-U-Th isotope data. United States Geological Survey. Open File Report: 88–557.

Malekpour, A., 2005. Petrofabrics and geochronology of the regional metamorphic rocks in the Aladdin and Molhedou mountains, SE of Shahrud, NE central Iran. M.Sc. thesis, University of Tehran, Iran (in Farsi, with English abstract).

Mallard, L.D., Rogers, J.J.W., 1997. Relationship of Avalonian and Cadomian terranes to Grenville and Pan_African events. Journal of Geodynamics 23, 197–221.

McDougall, I., Harrison, T.M., 1999. Geochronology and thermochronology by the $^{40}Ar/^{39}Ar$ method. Oxford University Press, New York.

McQuarrie, N., 2004. Crustal scale geometry of the Zagros fold–thrust belt, Iran. Journal of Structural Geology 26, 519–535.

Moritz, R., Ghazban, F., Singer, B.S., 2006. Eocene gold ore formation at Muteh, Sanandaj–Sirjan tectonic zone, western Iran: a result of late stage extension and exhumation of metamorphic basement rocks within the Zagros orogen. Economic Geology 101 (8), 1497–1524.

Murphy, J.B., Pisarevsky, S.A., Nance, R.D., Keppie, J.D., 2004. Neoproterozoic–Early Paleozoic evolution of peri-Gondwanan terranes: implications for Laurentia–Gondwana connections. International Journal of Earth Sciences 93, 659–682.

Nadimi, A., 2007. Evolution of the central Iranian basement. Gondwana Research 12 (3), 324–333.

Navai, I., 1987. Geological map of Khar Touran (scale 1:250,000), Geological Survey of Iran, Tehran, Iran.

Omrani, J., Khabbaznia, A.R., 2003. Geological map of Alut (scale 1:100,000), Geological Survey of Iran, Tehran, Iran.

Paces, J.B., Miller, J.D., 1993. Precise U-Pb age of Duluth Complex and related mafic intrusions, northeastern Minnesota: Geochronological insights into physical, petrogenic, paleomagnetic, and tectonomagnetic processes associated with the 1.1 Ga mid-continent rift system. Journal of Geophysical Research 98, 13,997–14,013.

Patchett, P.J., Chase, C.G., 2002. Role of transform continental margins in major crustal growth episodes. Geology 30, 39–42.

Parrish, R.R., 1987. An improved micro-capsule for zircon dissolution in U-Pb geochronology. Isotope Geoscience 66, 99–102.

Quidelleur, X., Grove, M., Lovera, O.M., Harrison, T.M., Yin, A., Ryerson, F.J., 1997. Thermal evolution and slip history of the Renbu Zedong thrust, southeastern Tibet. Journal of Geophysical Research 102, 2659–2679.

Rachidnejad-Omran, N., Emami, M.H., Sabzehi, M., Rastad, E., Belon, H., Pique, A., 2002. Lithostratigraphie et histoire paleozoique a Paleocene des complexes metamorphiques de la region de Muteh, zone de Sanandaj–Sirjan (Iran meridional). Comptes Rendus Geosciences 334, 1185–1191.

Ramezani, J., 1997. Regional geology, geochronology and geochemistry of the igneous and metamorphic rock suites of the Saghand region, central Iran. Ph.D. thesis, Washington University, St. Louis, Missouri, USA.

Ramezani, J., Tucker, R.D., 2003. The Saghand region, central Iran: U-Pb geochronology, petrogenesis and implications for Gondwana tectonics. American Journal of Science 303, 622–665.

Roddick, J.C., Loveridge, W.D., Parrish, R.R., 1987. Precise U-Pb dating of zircon at the sub-nanogram Pb level. Chemical Geology 66, 111–121.

Rogers, J.J.W., Unrug, R., Sultan, M., 1995. Tectonic assembly of Gondwana. Journal of Geodynamics 19, 1–34.

Ruttner, A.W., 1993. Southern borderland of Triassic Laurasia in north-east Iran. Geologische Rundschau 82, 110–120.

Samani, B.A., 1988. Metallogeny of the Precambrian in Iran. Precambrian Research 39, 85–106.

Samani, B.A., Zhuyi, C., Xuetao, G., Chuan, T., 1994. Geology of Precambrian in central Iran: on the context of stratigraphy, magmatism and metamorphism. Geosciences Quarterly 3 (10), 40–63 (Geological Survey of Iran, in Farsi with English abstract).

Sanudo-Wilhelmy, S.A., Flegal, A.R., 1994. Temporal variations in lead concentrations and isotopic composition in the Southern California Bight. Geochimica et Cosmchimica Acta 58, 3315–3320.

Schmitt, A.K., Grove, M., Harrison, T.M., Lovera, O.M., Hulen, J., Waters, M., 2003a. The Geysers–Cobb Mountain magma system, California (Part 1): U-Pb zircon ages of volcanic rocks, conditions of zircon crystallization and magma residence times. Geochimica et Cosmochimica Acta 67, 3423–3442.

Schmitt, A.K., Grove, M., Harrison, T.M., Lovera, O.M., Hulen, J., Waters, M., 2003b. The Geysers–Cobb Mountain Magma System, California (Part 2): timescales of pluton emplacement and implications for its thermal history. Geochimica et Cosmchimica Acta 67, 3443–3458.

Sengör, A.M.C., 1987. Tectonics of the Tethysides: Orogenic collage development in a collisional setting. Annual Review of Earth & Planetary Sciences 15, 213–244.

Sengör, A.M.C., 1990. A new model for the late Palaeozoic–Mesozoic tectonics evolution of Iran and implications for Oman. In: Robertson, A.H.F., Searle, M.P., Ries, A.C. (Eds.), The geology and tectonics of the Oman region, vol. 49. Geological Society of London Special Publication, London, pp. 797–831.

Stacey, J.S., Kramers, J.D., 1975. Approximation of terrestrial lead isotope evolution by a two-stage model. Earth and Planetary Science Letters 26, 207–221.

Stampfli, G.M., 2000. Tethyan oceans. In: Bozkurt, E., Winchester, J.A., Piper, J.D.A. (Eds.), Tectonics and magmatism in Turkey and surrounding area. Special Publication, vol. 173. Geological Society, London, pp. 1–23.

Stampfli, G.M., Borel, G.D., 2004. The TRANSMED transects in space and time: constraints on the Paleotectonic evolution of the Mediterranean Domain. In: Cavazza, W., Roure, F., Spakman, W., Stampfli, G.M., Ziegler, P. (Eds.), The TRANSMED Atlas: the Mediterranean Region from Crust to Mantle. Springer, pp. 53–80.

Stampfli, G.M., Mosar, J., Favre, P., Pillevuit, A., Vannay, J.C., 2001. Permo-Mesozoic evolution of the western Tethys realm: the Neotethys East-Mediterranean basin connection. In: Ziegler, P.A., Cavazza, W., Robertson, A.H.F., Crasquin-Soleau, S. (Eds.), Peri-Tethys Memoir 6: Peri-Tethyan rift/wrench basins and passive margins. Mémoires du Museum national d'Historie naturelle, vol. 186, pp. 51–108.

Steiger, R.H., Jager, E., 1977. Subcommission on Geochronology: convention on the use of decay constants in geo- and cosmochronology. Earth and Planetary Science Letters 36, 359–362.

Stern, R.J., 1994. Arc assembly and continental collision in the Neoproterozoic east African orogen: Implications for the consolidation of Gondwanaland. Annual Review of Earth and Planetary Sciences 22, 319–351.

Stockli, D.F., Hassanzadeh, J., Stockli, L.D., Axen, G.J., Walker, J.D., Dewane, T.J., 2004. Structural and geochronological evidence for Oligo-Miocene intra-arc low-angle detachment faulting in the Takab–Zanjan area NW Iran. Geological Society of America Abstracts with Programs 36 (5), 319.

Stöcklin, J., 1968. Structural history and tectonics of Iran: a review. American Association of Petroleum Geologists Bulletin 52, 1229–1258.

Stöcklin, J., 1974. Possible ancient continental margin in Iran. In: Burk, C.A., Drake, C.L. (Eds.), The geology of continental margins. Springer, pp. 873–887.

Stöcklin, J., Eftekharnezhad, J., 1969. Explanatory text of the Zanjan quadrangle map. Geological Survey of Iran, Tehran, Iran.

Stöcklin, J., Nabavi, M., Samimi, M., 1965. Geology and mineral resources of the Soltanieh mountains (Northwest Iran). Geological Survey of Iran, Tehran, Iran.

Stöcklin, J., Ruttner, A., Nabavi, M., 1964. New data on the Lower Paleozoic and Pre-Cambrian of north Iran. Geological Survey of Iran, Tehran, Iran.

Stöcklin, J., Setudehnia, A., 1970. Stratigraphic Lexicon of Iran. Geological Survey of Iran, Tehran, Iran.

Thiele, O., Alavi, M., Assefi, R., Hushmandzadeh, A., Seyed-Emami, K., Zahedi, M., 1968. Explanatory text of the Golpaygan quadrangle map. Geological Survey of Iran, Tehran, Iran.

Tillman, J.E., Poosti, A., Rossello, S., Eckert, A., 1981. Structural evolution of Sanandaj–Sirjan Ranges near Esfahan, Iran. American Association of Petroleum Geologists Bulletin 65, 674–687.

Veevers, J.J., 2003. Pan-African is Pan-Gondwanaland: oblique convergence drives rotation during 650–500 Ma assembly. Geology 31, 501–504.

Verdel, C., Wernicke, B.P., Ramezani, J., Hassanzadeh, J., Renne, P.R., Spell, T.L., 2007. Geology and thermochronology of Tertiary Cordilleran-style metamorphic core complexes in the Saghand region of central Iran. Geological Society of America Bulletin 119, 961–977.